UNIVERSIDADE DE SÃO PAULO
ESCOLA POLITÉCNICA
DEPARTAMENTO DE ENGENHARIA METALÚRGICA E DE MATERIAIS

ARTHUR DA ROCHA ALBERTINI

Protectivity of Mineral Deposits on Metallic Materials in the Context of the Development of New Geothermal Energy Sources

SÃO PAULO
2022

ARTHUR DA ROCHA ALBERTINI

Protectivity of Mineral Deposits on Metallic Materials in the Context of the Development of New Geothermal Energy Sources

Trabalho de conclusão de curso apresentado à Escola Politécnica da Universidade de São Paulo (EPUSP) para obtenção do título de Bacharel em Engenharia de Materiais em parceria com o *Institut National des Sciences Appliquées - Lyon* através do programa de Duplo Diploma.

São Paulo
2022

ARTHUR DA ROCHA ALBERTINI

Protectivity of Mineral Deposits on Metallic Materials in the Context of the Development of New Geothermal Energy Sources

Trabalho de conclusão de curso apresentado à Escola Politécnica da Universidade de São Paulo (EPUSP) para obtenção do título de Bacharel em Engenharia de Materiais em parceria com o *Institut National des Sciences Appliquées - Lyon* através do programa de Duplo Diploma.

Área de Estudo: Corrosão e Proteção de Superfícies Metálicas

Orientador: Dr. François Ropital
Co-orientadora: Dra. Sabrina Marcelin

Responsável EPUSP: Dr. Hercílio Gomes de Melo

São Paulo
2022

Projet de Fin d'Études

Protectivité des Dépôts Minéraux Sur les Matériaux Métalliques Dans le Cadre du Développement de Nouvelles Sources d'Énergie Géothermiques

Protectivity of Mineral Deposits on Metallic Materials in the Context of the Development of New Geothermal Energy Sources

Arthur da Rocha Albertini

July 2022

I, Arthur da Rocha Albertini, authorize the total or partial reproduction and dissemination of this work, by any conventional or electronic methods, for studies and research purposes; as long as properly cited.

I, Hercílio Gomes de Melo, responsible for this work, authorize the publication of this final version of this work in the USP library for scientific dissemination purposes.

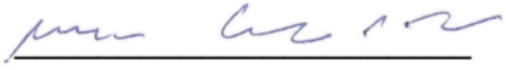

I, François Ropital, supervisor of this work, authorize the publication of this final version of this work in the USP library for scientific dissemination purposes.

Villeurbanne 01 August 2022 

Catalogação-na-publicação

Albertini, Arthur da Rocha
Protectivity of Mineral Deposits on Metallic Materials in the Context of the Development of New Geothermal Energy Sources / A. R. Albertini -- São Paulo, 2022.
75 p.

Trabalho de Formatura - Escola Politécnica da Universidade de São Paulo. Departamento de Engenharia Metalúrgica e de Materiais.

1.Corrosão 2.Deposição Mineral 3.Incrustação Acelerada 4.Inibidores de Corrosão 5.Usinas Geotérmicas I.Universidade de São Paulo. Escola Politécnica. Departamento de Engenharia Metalúrgica e de Materiais II.t.

Acknowledgements

It is important to show my most sincere thanks to the many people and entities that helped directly and indirectly during this graduation work.

First of all, I would like to thank my family, especially my parents (Cibeli and José Álvaro) and my brother (Álvaro) who, throughout my journey in France, gave me a lot of support and encouragement. In addition to all the efforts they made to make my studies in France possible.

Secondly, I would like to thank the CorrIs laboratory and all its staff, especially my advisors - Professor Doctor François Ropital and Doctor Sabrina Marcelin - who did their best to ensure that the work was delivered with relevance and quality, despite the difficulties caused by Covid-19.

In the same line, my great thanks to Benjamin Fornacciari and Sandrine Cardinal, who trained me in the use of the scanning electron microscope (SEM) and the X-Ray Diffractor (XRD) respectively.

Another group of people that I am very grateful for is the personnel of the Material and Metallurgical Engineering Department of the Polytechnic School of University of São Paulo. From teachers to technicians, all the employees have their share of help in my trajectory and they are recognized here.

I would like to especially thank Professor Doctor Guilherme Lenz, who started me in the research area through my scientific initiation, making me love research in the field of Materials Science. Also with whom I went to Russia to participate in the Metal Cup with five other students. Team for which I will take for a lifetime, I thank each of you also for all the support given and the company experienced.

The next thanks go to my college colleagues, both in Brazil and in France. During my college years it was increasingly evident how important these friendships were in my personal trajectory. More precisely, I thank you for the company and help from Milena and Luiza, brazilian students who came with me to do the double degree program in material science and engineering at INSA Lyon.

I am grateful for the great friends I made at CMR (Academic Center for Metallurgical, Materials and Mining Engineering in POLI - USP Brazil) that welcomed me and helped me so much in different moments of stress and joy.

I also want to thank all the other Brazilians who came to INSA Lyon to venture on a Double Degree or an Exchange journey. These people are so special that today I consider them a family.

I am very grateful to everyone, in this work and in my trajectory there is a little bit of each one of you.

RESUMO

Os Campos Geotérmicos são potenciais fontes de energia limpa (sem emissão de carbono) e, nos últimos anos, a área vem experimentando um grande crescimento. Um dos principais desafios para o seu desenvolvimento diz respeito à confiabilidade dos equipamentos em serviço, principalmente problemas relacionados à corrosão. De fato, as condições de operação em que o equipamento está inserido são muito agressivas. Os fluidos geotérmicos são carregados com compostos minerais e compostos extremamente oxidantes que podem gerar quantidades significativas de depósitos minerais nas superfícies metálicas da tubulação que, entre outros problemas, aumentam o risco de corrosão.

O processo de deposição mineral em superfícies metálicas é chamado de incrustação (scaling). Existem várias maneiras de simular e acelerar este processo, o método utilizado durante este trabalho consiste em acelerá-lo eletroquimicamente. A primeira parte do trabalho (em continuação de um trabalho feito anteriormente) foi finalizar a criação dos protocolos de teste e otimizar os testes de incrustação eletroquimicamente acelerados.

Uma vez que a deposição mineral, que normalmente ocorre na maioria das usinas geotérmicas, tem impacto negativo nas suas interferências (corrosão, entupimento de dutos, sobrecarga de tubulações), este trabalho teve como objetivo o melhor entendimento do funcionamento dos inibidores de incrustação. Para isso, foram testadas as relações entre um eletrólito semelhante a fluidos geotérmicos. Testes comparativos foram feitos com três inibidores diferentes em diferentes concentrações: soluções de HEDP, de Ferrofos 8450 e de TurboDispin 4363.

Foram obtidos resultados muito interessantes que comprovam a eficácia dos três inibidores testados, apesar de atuarem de formas diferentes. As concentrações de inibidores nas soluções mostraram-se um fator crucial para sua eficácia. Além disso, também foi estudada a relação (melhoria ou enfraquecimento) dos efeitos anticorrosivos para cada inibidor estudado, obtendo resultados muito diferentes para alguns deles.

Embora todos os três tenham um bom potencial como inibidor de incrustação, algumas concentrações não são recomendadas, pois elevam a taxa de corrosão a um nível alto.

Keywords: Incrustação Acelerada, Depósitos Minerais, Corrosão, Aço Carbono, Usinas Geotérmicas, Novas Fontes de Energia, Inibidores

ABSTRACT

Geothermal Fields are potential sources of carbon-free energy and it has been experiencing great growth in recent years. One of the main challenges for their development concerns the reliability of their equipment with regard to corrosion in service. Indeed, the operating conditions in which the equipment is inserted are very aggressive. The geothermal fluids are loaded with mineral compounds and oxidizing species which can generate significant amounts of mineral deposits on the metallic surfaces of the pipeline, among other problems, increasing the risk of corrosion.

The process of mineral deposition on metal surfaces is called scaling. There are several ways to simulate and accelerate this process, the method of accelerating it electrochemically was used during this work. The first part of the work (in continuation of an old work done previously) was to finalize the creation of the test protocols and to optimize the electrochemically accelerated scaling tests.

Since the mineral deposition that usually occurs in most geothermal plants has a negative impact in most of its interferences (corrosion, duct clogging, pipes overloading), this work aimed at the better understanding of the functioning of scaling inhibitors. For this, the relations between an electrolyte similar to geothermal fluids were tested. Comparative tests were made with three different inhibitors in different concentrations: HEDP solution, Ferrofos 8450 and TurboDispin 4363.

Very interesting results were obtained that prove the effectiveness of the three inhibitors tested, despite acting in different ways. The concentrations of inhibitors in the solutions proved to be a crucial factor for their effectiveness. In addition, the relationship (improvement or withering) of the anti-corrosion effects for each inhibitor studied was also studied, obtaining very different results for some of them.

Although all three have good potential as a scaling inhibitor, some concentrations are not recommended as they keep the corrosion rate at a high level.

Keywords: Accelerated Scaling, Mineral Deposits, Corrosion, Carbon Steel, Geothermal Power Plants, New Energy Sources, Inhibitors

LIST OF FIGURES

LIST OF TABLES

ANNEXED TABLES AND FIGURES

CONTENTS

1. Context of the Project

1.1. Corrosion Theoretical Introduction

Nowadays, corrosion is a major technical challenge faced in many different domains. Corrosion issues can cause high economic impacts for a company.

Corrosion can be defined in several ways: (1) destruction or deterioration of a material due to its reaction with its environment, (2) destruction of materials by means other than mechanical or (3) the reverse of metallurgy extractive. But according to the ISO 8044 standard, widely used in the field of metallurgy, corrosion is defined as "the physicochemical interaction between a metal and its surrounding environment leading to modifications in the properties of the metal and possibly leading to a significant degradation of the function of the metal, of the surrounding environment or of the technical system of which they are part".[1]

The consequences of corrosion can lead to aesthetic problems, but more importantly, corrosion can lead to compromised functionality of an entire structure. In addition, corrosion poses a very high risk for many stages of a process in which metallic materials are involved.

The treatments related to corrosive phenomena (for example, corrosion prevention and restoration or exchange of corroded parts) have a significant economic impact in many processes. It is estimated that the direct (exchange of corroded equipment and materials) and the indirect (low productivity and time spent connected) expenses related to corrosion represent about 4% of the total expense of an entire product.[2]

Therefore, we conclude that large companies have a major interest in avoiding this type of risk and loss as much as possible.

1.2. Exploration of Geothermal Sources

With the possible shortage of fossil fuels and growing concerns about the environmental problems they cause, the use of renewable energy sources tends to increase and diversify. Geothermal Energy, defined briefly as thermal energy from the Earth's interior, may be able to help solve some of these current energy and environmental problems, and may, in the future, become a fundamental resource to make society more sustainable.[3]

During the Earth's natural cooling process, internal heat can be dissipated anywhere on the Earth's surface. However, there are regions where the release of this heat is more intense, usually coinciding with active zones on the borders of the tectonic plates of the globe. It is in these areas that the largest energy generation geothermal plants in the world are located.

The exploitation of this energy source is not new, but it remains less known and used than other renewable energies, such as hydroelectric, wind energy or photovoltaic. However, there are several important advantages that justify the recent growth of the sector. First, the production of heat or electricity by geothermal plants has a low environmental impact and the greenhouse gas emission rate is really low when compared to many current energy sources. Furthermore, the Earth's heat is not an intermittent source, i.e. it is available continuously (unlike sources such as wind and solar).

The use of thermal energy from the innermost layers of the Earth can already be done in different ways: (1) district heating of individual houses or companies with the aid of a heat pump, (2) heating crops in greenhouses or fish farming tanks, (3) heat network that supplies urban areas, with heating and domestic hot water, (4) production of electricity in geothermal plants. Regarding this latest use, although still small on a global scale, it represents an important part of the electricity mix in some countries such as Kenya, Turkey, Indonesia and Iceland for example. With technical advances in the sector, there is an increase in the efficiency in the production of electric energy and its use has been increasing as shown in figure 1, mainly in geologically unfavorable areas. This is happening because nowadays it is possible to explore such resources in new areas thanks to new exploration techniques, for example hydraulic fracturing (technique used in France at the Soultz-sous-Forêt plant).

The technical know-how achieved already allows us to produce electricity at costs comparable to those of other renewable energies (hydroelectric and wind energy) and to generate heat at competitive costs compared to the one produced by fossil fuels (gas and oil).

1.2.1. Geothermal Sources in France

French legislation divides geothermal energy into three basic sectors according to their origin: (1) High Temperature, geothermal fluids with temperatures greater than 150°C, (2) Low Temperature, fluids below 150 ° C and (3) the called geothermal energies of minimal importance, coming from depths less than 200m and production potentials less than 500W.[5]

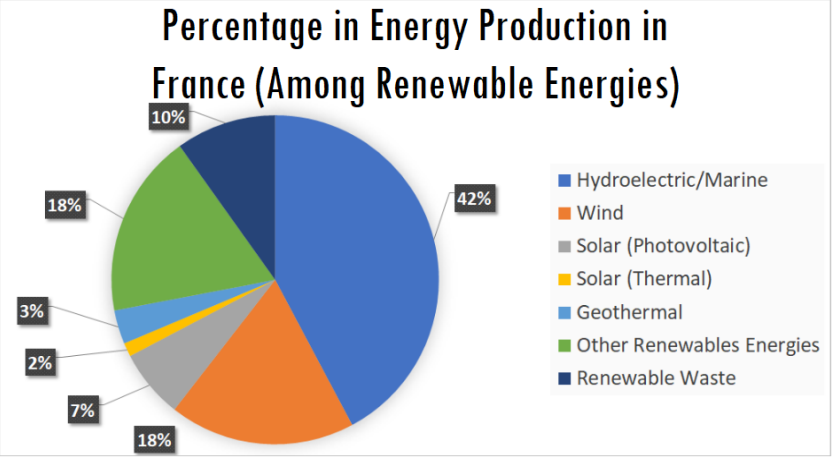

Figure 1: Importance of Geothermal Energy in France
Source: IRENA (Renewable energy statistics 2020) [4]

1.2.2. Geothermal Sources in Brazil

The feasibility of using geothermal energy in Brazil is still discussed, requiring studies that reveal the real potential for applying this type of energy in Brazil.

Investments are currently being discussed, mainly regarding the exploitation of the geothermal potential of the Guarani Aquifer, whose water temperature may even be able to heat the water of buildings or houses and heating systems and fireplaces. But more recent studies show that the expectation for the coming years is that the use of heat pumps will become common in Brazilian cities.

Although there are no large-scale geothermal energy plants in Brazil, their future use as heating systems in cities in the south-southeast of the country, close to the Guarani Aquifer, is promising. In addition, the knowledge acquired in this study can be used to avoid scaling in many types of piping, for example those used in water distribution systems or in fuel pipelines.

In Brazil, the transportation of fluids through pipelines is the main means used by oil, gas and sanitation companies. The buried metal ducts are subject to external and internal corrosion, influenced by several factors: type of material used in the manufacture of the duct, characteristics of the soil and lining, action of interference currents, among others.[7] The scaling and corrosion inhibitors tested in this work could also be useful in those cases.

Just for the sake of comparison, the percentage corresponding to renewable energies was around 19.1% of the gross energy consumed in France [33]. While, in Brazil, this number rises to around 45.0%.[34]

1.3. Geothermal Energy: Why hasn't it taken off yet?

Despite being a relatively cheap and reliable renewable source, the extraction of heat from terrestrial magma is exclusive to few countries (in relevant values). But dozens of countries have untapped potential, which is estimated today to be around 200 gigawatts.

Political leaders from 25 countries met in 2017 in Florence, Italy, hoping to change the scenario of the low use of geothermal energy in the world. The government ministers and 29 partner institutions present there signed the "Florence Declaration", in which everyone pledged to obtain a 500% increase in the global installed capacity for geothermal energy generation by the year 2030.

Although the percentage sounds high, it applies to a very modest initial figure, since currently geothermal energy only accounts for 0,3% of the global installed capacity (2017). However, the potential of this type of renewable energy generation is enormous, both to reduce greenhouse gas emissions and to reduce costs. And we can see on Figure 2 the global installed capacity is growing fast the last few years.

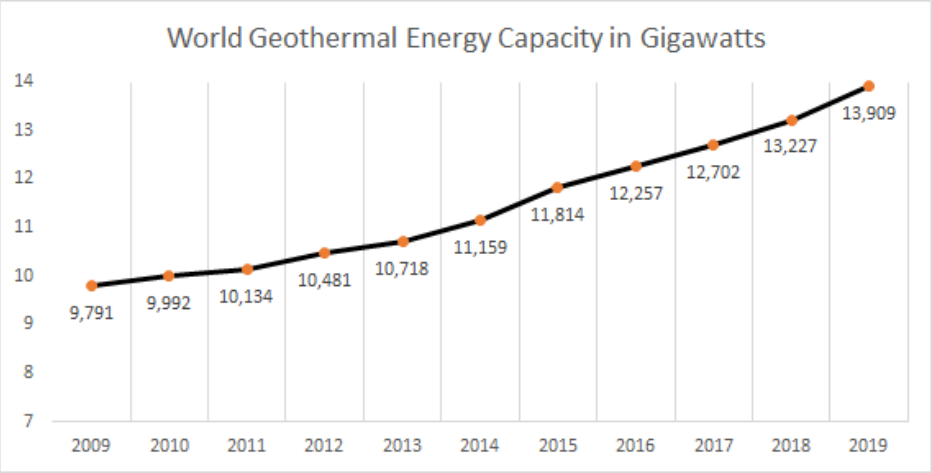

Figure 2: Growing Geothermal Energy Capacity in the World
Source: IRENA (Renewable energy statistics 2020) [4]

"To use this advantage, the operational availability of geothermal energy installations has to be stable on a high level. Scalings and material corrosion for instance, are issues in many geothermal areas in Europe. Both lead to breakdown times due to necessary repair or service works. Also other issues like high gas content of the thermal brine or pressure related issues have to be controlled for continuous availability of the resource." [5]

2. Corrosion in Geothermal Field

2.1. Problems linked to Corrosion

Even with such potential for growth, geothermal power plants have operational problems in their facilities that can act as a barrier to the production of a reliable and safe energy.[5] Among these operational barriers, corrosion is a major cause for the degradation of metallic materials. In the equipment of this type of plant, corrosion is intensified due to the geothermal fluids enriched with extremely aggressive solutes.

Studies show that a geothermal plant is designed for at least 20 years of operation without major equipment maintenance. To meet this demand, an area of extreme importance during the study and design of the plant is the choice of materials for all the machinery and equipment of the facility.[6]

Massive plant equipment failures caused by corrosion have been reported in many geothermal facilities. As already shown, corrosion can basically be described by the destruction of a material due to (electro)chemical reactions with the surrounding environment (and it also could be triggered and worsened by mechanical stress). In the geothermal field, most components that are in contact with geothermal fluids are made of steel because of their high mechanical stability at high pressures and temperatures. Some of these materials can develop a thin (hydro-)oxide film on their surfaces, called passive or pseudo-passive film, which prevents them from general corrosion.

However the problem is that geothermal fluids contain a lot of chlorides, for example, that turns the environment a lot more aggressive for most materials, because they can even deteriorate those (pseudo-)passivation layers over time.

2.2. Geothermal Fluids

To understand the phenomenon of corrosion in geothermal equipment, it is first necessary to know the composition of the fluids. Generally, the composition of those fluids is known only in the drilling phase and is often complex. In addition to the presence of a large number of salts and species dissolved in the aqueous phase, the gases are also present in the dissolved form. Temperature and pressure are also very important data that can influence the process. In fact, variations in these two parameters cause changes in fluid properties (mineral precipitation, pH variation, etc.) that have a direct effect on the corrosion phenomenon.

In these environments it is impossible to generalize the corrosion phenomena, because the fluids are different depending on where they are on the planet. However, it is possible to report trends of more or less corrosive fluids. Recently, *Nogara and Zarrouk et al* [8] published an article classifying some of these fluids according to their degree of corrosivity. In Table 1, fluids are listed in decreasing order of corrosivity. This classification is based on TKS (Total Key Species), which represents the sum of the relative masses of species identified as responsible for corrosion: chlorides, sulfates, CO_2, bicarbonates, carbonates and ammoniacal species. There are, in the annexed table 1, more details of each class of fluid.

Table 1: Classification of geothermal fluids according to their corrosivity [8]

Classification	Characteristics	TKS ($g.L^{-1}$)	pH	Plants Examples
I	Hyper saline fluid at acidic pH	>100	<5	Salton Sea (USA)
II	Saline fluid at acidic pH	1 - 100	3 - 5	Soultz-Sous-Forêts (France)
III	Saline fluid at neutral pH	10 - 20	5 - 6	Cerro Prieto (Mexico)
IV	Moderately saline fluid at neutral pH	0,5 - 10	5 - 6	Ahuchapan (El Salvador)
V	Low saline fluid at basic pH	<5	>7	Bassin Molassique (Austria)

In fact, the classification of these fluids is complex because there is a large number of them and they are very different and specific. It is a useful tool, to simplify the choice of materials, by referring to the mineral scales that can deposit with similar fluids. The main criteria for the classification proposed by J. Nogara and SJ Zarouk are: (1) the phase(s) present, (2) the temperature and pressure conditions (3) the speed of the fluids, (4) the pH, (5) the quantity of corrosive species present and (6) mineral species present which can lead to mineral deposits.[8]

2.3. Material Selection for Geothermal Plants

As already shown, a major problem for geothermal plants is the corrosion of the plant equipment. The geothermal water which is extracted in these areas to generate electricity comes from a depth between 1500 and 5000 meters. Those brines are in equilibrium with its surrounding ground. Different amounts of dissolved substances like chloride, hydrogen sulfide and carbon dioxide which are highly corrosive could be present.[3][8][9]

It is a big challenge to select construction materials which serve their mechanical purpose and are adequate for the use in a corrosive environment. Since the service life of plants is estimated to be at least 20 years, materials must be stable over a long period of time.

Metallic materials are the most chosen ones when it comes to equipment for geothermal power plants, especially those that are directly in contact with geothermal fluids. This choice is due to the exceptional characteristics and properties that this type of material can possede.[6]

Heat exchangers, for example, are made of metallic materials because of their excellent thermal conductivity. Pipes and valve systems are made of metallic materials due to their strength, hardness and ease of processing. Furthermore, most of the time, metallic materials have a very competitive price in relation to other types of more specific materials.

Basically, the selection of material depends on the chemical and mechanical characteristics of the environment that it will be inserted in and also on the purpose of its use. But never forgetting its value and its lifetime in use.[6]

2.3.1. Carbon Steel

Most of the tubing of geothermal plants is made of carbon steel.[9] Although they do not have a great resistance against the generalized corrosion of geothermal brines and do not form a passive film on their surface for protection, this choice happens because of their high resistance to fracture (generally higher than that of ferritic and austenitic stainless steels), in addition to very competitive price (much lower than duplex steels for example).

A good control of the corrosion rate of carbon steels are the corrosive deposits on its surface that may (or may not) protect against the continuation of the corrosion process.

Typical carbon steels that are used for coating and piping in geothermal water are API L80, API P110, API Q125, XC42, XC38 and P265GH[10] (compositions are presented in the annexed table 2). They mainly differ from each other by their carbon content and their mechanical properties, with the exception of L80 steel, which has a high amount of chromium in its composition, but it is worth mentioning that this steel is not used much due to the aggressive environment already mentioned.

For tasks designated for piping it is not necessary to keep the pipe surface very uniform and a moderate uniform corrosion rate is allowed, which is why the use of carbon steel is very plausible here. The common limit for the corrosion rate is set at a maximum of ***0.3 mm/year***.[11]

On the other hand, it is not possible to allow the uniform corrosion for functional components such as heat exchangers, valves and pumps because its functionality could be compromised. For such kinds of applications it is necessary to think a little bit more about the corrosion resistance of the material. The most common materials for those uses are highly corrosion resistant stainless steels, nickel-based alloys and even titanium materials.

2.3.2. *Stainless Steel*

Stainless steels are ferrous materials that have alloy elements in relevant quantities in their composition, mainly metals such as chromium, nickel, molybdenum, manganese and niobium. The main element to be observed when formulating a stainless steel is chromium. The main differential of this type of material is that they form a layer of chromium oxide on the surface, if the chromium content is greater than 10,5% (the passive film). This layer separates the metal surface and the atmosphere, protecting it from further dissolution.

Corrosion is strongly decelerated due to the passive film and uniform corrosion is no longer a risk, as the steel surface is not directly exposed to its surroundings. But components present in geothermal fluids can attack this oxide layer like halogen ions (for example chlorides, Cl^-) or sulfide ions, making possible the beginning of processes that we call localized corrosion, those are types of corrosion that are very dangerous and that can lead to the metal to corrode and its function to be compromised.

It is known that the carbon contents in stainless steels are low (greater protection against corrosion), this can lead to mechanical problems in certain applications. After the steel cool-down the small amount of carbon is concentrated in its grains boundaries. This carbon concentration makes the steel susceptible to intercrystalline Stress Corrosion Cracking (SSC), that means the despite many times invisible with human unaided eyes, there will be corrosion in the grain boundaries and the steel will be more fragile to intergranular rupture. The reason for other alloying elements, like titanium and niobium in its composition is to form carbides aiming for the stabilization of stainless steel with very low carbon contents.

Other components can be added to the alloy with the main goal of changing its microstructure. There are elements that are ferrite formers (like chromium, molybdenum, titanium,niobium, tungsten, vanadium, silicon and aluminium).[9] Meanwhile alloying elements which form austenitic structures are nickel, carbon, copper, nitrogen, cobalt and manganese.[9] The annexed table 3 has the aiming goal for each of those alloy elements used in stainless steels.

There are also more corrosion resistant steels that mix the two microstructures, they are called the duplex stainless steel. Duplex steels consist of a mixture of ferritic and austenitic mixed crystals. These steel types have the highest yield strength among the stainless steels with high corrosion resistance and they have also good values for toughness.[13]

However, in temperatures higher than 100 - 150 °C its corrosion resistance abruptly drops below values of austenitic steels. The reason for this behavior is probably the low stability of the microstructure because the austenitic and ferritic structures are very different.[14]

In high temperatures, the austenitic phase gets poor of chromium and molybdenum atoms and loses its corrosion resistant character. Furthermore, at temperatures of about 300 – 450°C a transition phase happens while the strength and the corrosion resistance decreases even more.

At those temperatures, the intermetallic precipitation of FeCr is accelerated leading to the chromium depletion explained above. As a consequence of this it is necessary to use carbon steel or austenitic steels with a nickel content higher than 25% in high corrosive brines at elevated temperatures.[14]

2.4. Types of Corrosion Found in Geothermal Plants

Different types of corrosion have been and are frequently observed in geothermal installations. The table 2, extracted from a manual of reports of problems registered in geothermal plants,[5] shows in detail not only the types of corrosion found, but also the main factors that trigger each type of corrosion.

Table 2: Types of corrosion found in geothermal plants and their main causes[5]

Relevant Property in the Fluid	Corrosion Type	Process Details
High Concentration of Chlorides (Cl^-)	Pitting Corrosion	Interference with an alloy's ability to reform a passive film. Local fluctuations induced by high chloride concentrations can prevent the film formation. The degradation of the oxide film at a few critical points, can lead to the formation of corrosion pits.
High Proton (H^+) Content	Generalized Acid Corrosion	Low pH values result in material dissolution. The decrease of the fluid's pH value is induced by the formation of carbonic acid, precipitation of hydroxides, or artificially by fluid acidification.
CO_2	CO_2 Corrosion	Formation of hydro carbonic acid (acid corrosion) and carbonates as corrosion products.
H	Hydrogen Embrittlement	Hydrogen atoms diffuse through the metal and by recombination to hydrogen molecules creating pressure from within the metal resulting in cracks.
H_2S	Sulfide Stress Corrosion (SSC)	Reaction of steel with H2S: formation of metal sulfides and elementary hydrogen. The hydrogen diffuses into the metal matrix and continues damaging the material (effects of H2)
Oxidizing Ions (Dissolved More Noble Metals)	Electrochemical Corrosion	Metals dissolved (for example Cu^{2+} or Pb^{2+}) could be reduced at contact with materials of the installations (carbon steel), thereby the dissolved species precipitates and iron dissolves.
Temperature	-	Usually, higher the temperature, the faster will be the reaction.

2.4.1. Corrosion caused by geothermal water - Uniform (or generalized) acid corrosion

This kind of attack happens on the entire exposed metallic surface. It takes place at about the same rate of corrosion on the exposed surface. This is the most common form of corrosion but it is generally less dangerous than the others because it is possible to see the damage done to the material and also predict its failure.

This type of corrosion occurs when the corrosive environment has uniform access to the metal surface. Uniform corrosion is the result of electrochemical reactions. In the presence of CO_2, the uniform acid corrosion process can be summarized by 3 cathodic reactions (II to IV) and one anodic reaction (V) explained below. First, the gaseous CO_2 dissolves in water to form carbonic acid according to equation 1, which then corrodes the steel.

$$CO_{2\,(g)} + H_2O_{(aq)} \rightarrow H_2CO_{3\,(aq)} \quad \text{(I)}$$

3 Cathodic Reactions:

$$2H_2CO_3 + 2e^- \rightarrow H_2 + HCO_3^- \quad \text{(II)}$$

$$2HCO_3^- + 2e^- \rightarrow H_2 + 2CO_3^{2-} \quad \text{(III)}$$

$$2H^+ + 2e^- \rightarrow H_2 \quad \text{(IV)}$$

1 Anodic Reaction:

$$Fe \rightarrow Fe^{2+} + 2e^- \quad \text{(V)}$$

This group of reactions causes iron oxidation and then a thickness loss of the metal over time. For geothermal applications, it is considered that the corrosion rate is acceptable if it does not exceed the threshold value set at ***0.3 mm per year***.[9] This value indeed corresponds to a loss of thickness of **6 mm in 20 years** of service. Figure 3 shows a photograph of the uniform corrosion visible at the head of a geothermal well.

Figure 3: Generalized acid corrosion at the head of a geothermal well [8]

2.4.2. Corrosion caused by geothermal water - Pitting corrosion

Pitting corrosion is a highly localized form of corrosion, its damage can be seen in Figure 4(a), it occurs in stainless steels with defects in the oxide layer (the inner layer of a passive film) or in the inhomogeneity of the metal surface, which can induces defects in the passive film.[16]

Those defects play the role of anodes, while the passivated surface of the metal behaves like the cathode, leading to the electrochemical reaction in the exposed locations. This great area ratio, in favor of the cathode, causes very rapid and deep corrosion.[9] This happens if the pitting holes are active.

They could also be sometimes metastable, meaning that there is competition between the repassivation of the holes and dissolution of the metal. Corrosion products can also have the role of protection by "blocking" the spread of the pitting.

Furthermore, very high concentrations of aggressive anions, such as chloride ions or sulfate ions combined with low pH values, often caused by the presence of chlorides, CO_2 or H_2S, considerably increase the risk of pitting corrosion, as is the case with the geothermal installations that we are concerned about.

2.4.3. Corrosion caused by geothermal water - Crevice corrosion

This type of corrosion is similar to pitting corrosion but however more aggressive. The geothermal brines which stagnate in the crevices participate in the increase of the corrosive agents concentration, leading to locally destruction of the passivation layer. As we see in Figure 4(b), corrosion by crevice effect is limited to confined areas unlike pitting corrosion which takes place in any exposed area of the metal.

On the other hand, like pitting corrosion, it depends on the aeration of the electrolyte due to the geometry of the assembly (main factors are: the concentration of chloride and sulfides, the temperature, the presence of oxygen and the pH).[16]

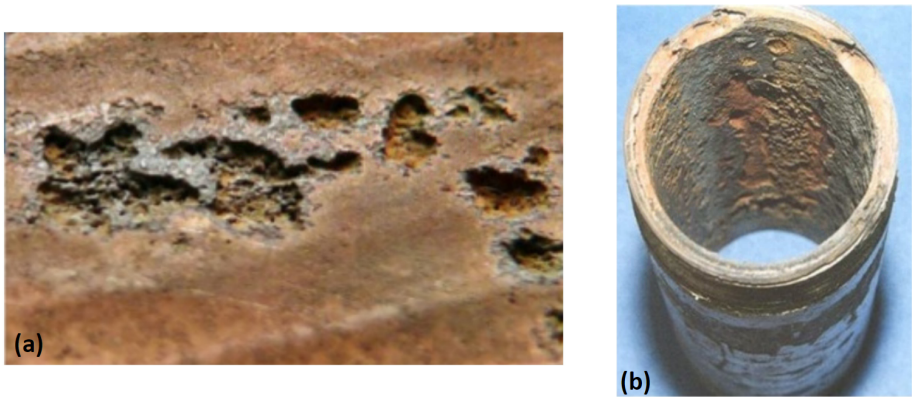

Figure 4: Effects of pitting (a) and crevice (b) corrosion on geothermal power plants equipments[16]

2.4.4. Corrosion caused by geothermal water - Galvanic corrosion

This type of corrosion occurs when two metals, with different electrochemical potentials, are brought into contact by an electrolyte. The metal with the lower potential (less noble) acts as an anode and oxidizes, while the other metal is the cathode, then it suffers reduction. In addition, if the anode area is smaller than the cathode area, the rate of dissolution of the less noble metal will be very high.

2.4.5. Corrosion caused by geothermal water - Stress corrosion cracking (SCC)

It comes from the combination of a mechanical stress in tension and an aggressive environment. This type of corrosion causes cracks perpendicular to the direction of stress propagation resulting in a failure. The stresses can be thermal, residual or in tension. It usually occurs in stainless steels with very small amounts of carbon.

2.4.6. Corrosion caused by geothermal water - Hydrogen Induced Cracking (HIC)

When the material is inserted in a media rich in H_2S, we then speak of corrosion induced by sulfide cracking. It occurs when the materials are in contact with brines containing H_2S. The hydrogen atom diffuses inside the metal and recombines at the defects of the metal to form molecular hydrogen (H_2) as a resultant element of the corrosive process reactions.

Blisters and bubbles appear on the surface of the metal. Hydrogen embrittlement significantly decreases the metal's ability to deform, making it really brittle.

2.4.7. *Corrosion caused by geothermal water - Corrosion by fatigue*

It differs from stress corrosion cracking in that the stresses are no longer static or constant but cyclical. High temperatures, acidity and the composition of the medium have an impact on the susceptibility of materials to this form of corrosion.

2.4.8. *Corrosion caused by geothermal water - Corrosion-Erosion*

This type of corrosion is caused by the relative movement between the corrosive fluid and the metal. Erosion-corrosion is amplified by turbulence phenomena and the speed of the fluid. This usually begins with a brutal destruction of the protective film, which then exposes the metal surface to the corrosive environment.

2.5. Role of chlorides in the pitting corrosion process

Most of the geothermal brines in Eastern Europe are classified as CO_2-rich NaCl waters. The concentration of Total Dissolved Solids can exceed 100 $g.L^{-1}$ and it is possible to consider that the chlorides are the most common anion present in it. We conclude that, from a corrosion point of view, there are two mechanisms to be most concerned of: (1) the CO_2 generalized acid corrosion, in combination with the (2) chloride-induced pitting corrosion.[15]

Chlorides are known by destroying and destabilizing oxide films on passivating metals, leading to localized pitting corrosion in stainless steels.[15] The mechanism triggered by chlorides is shown in figure 5.

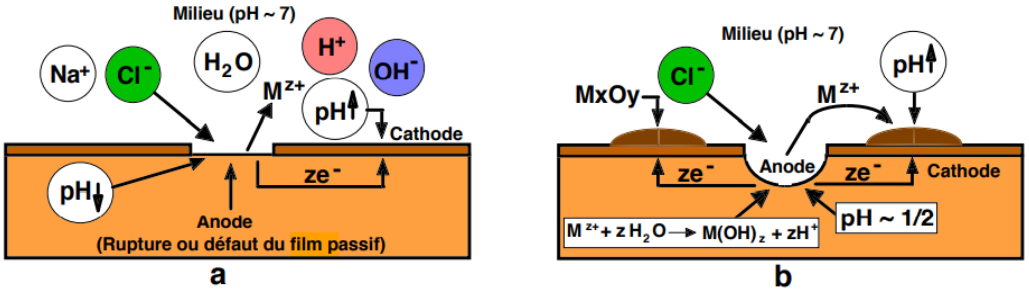

Figure 5: Pitting corrosion mechanism triggered by chlorides[20]

2.6. Why avoid Stainless Steels for those uses?

The main reason for avoiding those kinds of material in Geothermal Power plants lies in the composition of the geothermal fluids. More precisely it depends on the concentration of chlorides and other aggressive ions in its composition. Stainless steels in environments containing aggressive ions such as chlorides are liable to undergo localized corrosion. Those two kinds of corrosion are hard to predict and to quantify, leading to unexpected failures of equipements.

The pitting corrosion, for example, is one of the most destructive and insidious forms of corrosion. This causes equipment failure due to puncture with only a small percentage of weight loss of the whole structure. Sometimes it can be difficult to detect pits due to their small size and because pits are often covered with corrosion products. It is reiterated that this phenomenon is also difficult to predict by laboratory tests.

A study was carried out to better understand the critical concentration of chlorides that generate cracks in 316L stainless steel. Therefore, even though carbon steels are less resistant to generalized corrosion, they are widely used, in this case, due to their low cost, greater ease of predicting maintenance and less risk of unexpected failures.

2.7. Natural deposition of calcium carbonate

Natural waters contain a lot of ions, dissolved or suspended matter and dissolved gases. The composition of water is in a way determined by its history. This composition will indeed depend on the structure or geological structures in which the water has stayed but also on its surface path where it is in contact with the atmospheric sphere and where and how it can be polluted.

The most common mineral deposit in natural waters is composed mainly of calcium carbonate because it is a very poorly soluble salt and present in large quantities in most natural water reserves. The formation of those deposits depends on the concentration of dissolved CO_2, according to the chemical equations below:

$$CO_{2(aq)} + H_2O \Leftrightarrow H^+ + HCO_3^-$$

$$HCO_3^- \Leftrightarrow H^+ + CO_3^{2-}$$

$$Ca^{2+} + CO_3^{2-} \Leftrightarrow CaCO_{3(s)}$$

Several methods led to the heterogeneous crystallization of $CaCO_3$ onto various solid substrates. Under natural conditions, the process often takes a long time to start or become noticeable in the analysis. For scientific purposes, many methods have been developed to accelerate this process in order to be able to better study and understand them.

The idea of these methods are also variable, sometimes to study the scaling power of the solvent, the efficiency of a physical or chemical treatment to reduce scaling or simply to characterize the calcium carbonate deposits themselves under specific conditions. In short, it is used to obtain results more quickly and efficiently.

These methods can be thermal, chemical or electrochemical but all of them are based on the displacement of the calcium-carbon balance in the direction of the formation of calcium carbonate in the equilibrium equation below.

$$Ca^{2+} + HCO_3^- + OH^- \Leftrightarrow H_2O + CaCO_{3\,(s)}$$

With basic knowledge of physicochemistry we can determine several ways to shift the balance, favoring the formation of $CaCO_3$. Among those ways, it is possible to:

- Increase the concentration of Ca^{2+} and CO_3^{2-} ions by evaporating part of the solvent.
- Increase the pH by adding highly basic components (soda for example). This will increase the OH^- concentration in the solvent.
- Use a supersaturated solution obtained by mixing a solution of calcium chloride and a carbonate salt. The precipitation is then triggered by the increase in pH.
- Promote the deposition of $CaCO_3$ locally by promoting the oxygen reduction reaction to increase the pH in the vicinity of a surface (electrodeposition accelerated scaling method).

In this work, we will focus on the last method to accelerate the scaling process.

2.7.1. Electrodeposition Accelerated Scaling Method

For over a hundred years there have been studies that aim to understand and characterize the scale rate of some type of solvent containing mineral ions (mainly natural water). It is noticed that all the existing tests are based on the thermodynamic laws to displace the equilibrium equations in favor of the formation of the mineral deposit in question.

This method is not different. The main idea of this method is that the scaling can be accelerated by reducing the dissolved oxygen in the experience water according to the global electrochemical reaction:[21]

$$O_{2(aq)} + H_2O + 4e^- \rightarrow 4\,OH^-$$

This reduction leads to an increase of the local pH near the electrode, and the formation of hydroxide ions forces the calcium cations to precipitate in a solid phase according to the reaction (calcium carbonate):

$$Ca^{2+} + HCO_3^{2-} + OH^- \Leftrightarrow CaCO_{3\,(s)} + H_2O$$

The nature of the calcium carbonate precipitate depends on the temperature and the chemistry of the solution studied. Calcium carbonate comes in the form of three different polymorphs: calcite, aragonite, and vaterite.

Calcite is the most common form due to its stability at room temperature. Calcite is one of the forms of calcium carbonate that occurs in rhombohedral form. Aragonite is stable at high temperature and pressure and can therefore be more easily observed under these conditions. However, vaterite is a metastable intermediate form which is more rarely observed.

Usually, the calcium carbonate precipitates under the form of calcite and it is easily recognizable thanks to the cubic shape of the deposited crystals, which can be observed by scanning electron microscopy (SEM) but the calcite phase can also be detected by X-Ray diffraction.

The simplest and most used technique to investigate scaling processes is the chronoamperometry test. This method will be explained in subsequent parts but the progressive blocking of the electrode active surface by $CaCO_3$ crystals can be detected by the decrease of the current intensity with time.

2.7.2. PHREEQC Software

PHREEQC stands for **PH RE**dox **EQ**uilibrium (in **C** language), it is a computer program written in the C++ programming language that is designed to perform a wide variety of aqueous geochemical calculations. With this program it is possible to simulate chemical reactions and transport processes in a wide variety of aqueous solutions.

For our study the most important feature of this program is its capacity to calculate saturation indices and predict what are the mineral deposits most likely to occur in each case. Before starting the experimental phase, studies made in PHREEQC by another group of students showed the most likely to occur mineral deposits of Calcium Carbonate for different solutions (being the most important factor the Ca^{2+} concentration and the temperature of the solution-sample set).[28]

Table 3: Prediction of precipitation for different solutions at different temperatures using the PHREEQC software[28]

Solution (Water Type)	Calcium Content	T = 25°C	T = 50°C	T = 100°C
Synthetic Solution	1300 mg/L	Aragonite, Calcite	Aragonite, Calcite	Aragonite, Calcite
Hepar Water	550 mg/L	Aragonite, Calcite, Dolomite	Anhydrite, Aragonite, Calcite, CO_2, Dolomite, Gypsum	Anhydrite, Aragonite, Calcite, CO_2, Dolomite, Gypsum
Evian Water	78 mg/L	-	Aragonite, Calcite, CO_2, Dolomite	Anhydrite, Aragonite, Calcite, CO_2, Dolomite
Volvic Water	12 mg/L	-	-	-

Analyzing table 3, it is clear to note that the type of precipitation is strongly linked to the calcium content of the different solutions. In short, the higher the calcium content, the easier mineral deposits will take place at low temperatures.

Volvic water was the most "pure" solution tested by them and the result of the prediction is that there would be no deposition even at 100°C, which is not necessarily true as will be shown later in this work. It happens probably because the software does not take into account the kinetic aspect of scaling and only simulates precipitation as a function of the concentrations and of the pH and temperature conditions.

Another important and interesting feature that the software can calculate is the saturation indices as a function of temperature by modeling. This calculation helps to determine the extent of the scaling. It is negative for an undersaturated solution, zero for a saturated solution and positive when the solution is supersaturated.

It is calculated by determining the ratio of the chemical activity product of the ions to the equilibrium constant K of the corresponding salt, as shown by the equation below.[28]

$$SI_{CaCO_3\ at\ T°C} = log\frac{(Ca^{2+})\cdot(CO_3^{2-})}{K_{(CaCO_3)\ at\ T°C}}$$

The solubility of salts and, therefore, the saturation index of a solution, are parameters that depend on factors such as temperature, pressure, pH, etc.

2.8. Scaling and its influence in the corrosion process

In addition to the components of geothermal brines that directly affect the reaction process, there are also elements that may deposit on the metallic surface, indirectly interfering with corrosion reactions; this deposition of mineral compounds is called scaling.

In fact, the scaling process, in the field of geothermal industries, is the expression that defines and explains the precipitation of solids present in brines due to supersaturation or influenced by electrochemical processes (redox).

The most commons scaling deposits in geothermal brines are: **(1)** carbonates {$FeCO_3$ (siderite), $CaCO_3$ (calcite), $CaMg[CO_3]_2$ (dolomite)}; **(2)** sulfates and sulfites {$BaSO_4$ (barite), $SrSO_4$ (celestine) or PBS (galena), ZnS (sphalerite)}; **(3)** native metals {Pb (lead), Zn (zinc), Cu (copper)}; **(4)** metallic and other inorganic compounds {$Al(OH_3)$, SiO_2 (quartz), Fe_3O_4 (magnetite)}.[9]

These scalings precipitate due to electrochemical reactions and changes in water conditions (pressure and temperature for example). Taking into account the composition of brines and the most used steels (carbon steel), it is possible to predict that the most common types of mineral deposition are the ones with calcium.

With those deposits, a protective layer made of calcite ($CaCO_3$) and siderite ($FeCO_3$) can be formed on carbon steel in specific conditions. This layer can provide protection of the component if the layer is adherent to the substrate and compact. But if not, it can be a facilitator to concentrate gases and other elements in the voids between the metal surface and the mineral oxide layer, which can lead to crevice corrosion for example. It is important to remind that the microstructure of the corrosion product depends on the temperature and pressure of the formation and the nature of the substrate material.[15] High pressure can have a positive effect on the layer because it becomes even denser.

However, there are studies showing that the calcite-siderite layers which form from the water composition in the Central European geothermal locations may not prevent corrosion but it can at least slow down the process.[9][15]

But in the case of metal deposits or if there are defects in the mineral layers, a galvanic coupling between covered and uncovered regions can be established and localized corrosion is likely to occur.[15]

Mundhenk et al.[15] discovered that the corrosion rate of carbon steel in thermal water is lower at higher temperatures, that is another reason why this kind of steel is used in these applications. They showed that at high temperatures, carbon steel corrodes strongly and many Fe ions dissolve. Quickly, a dense layer of siderite is formed due to the large number of dissolved Fe ions, delaying the corrosion process; this effect can be even greater if combined with the formation of calcite. It is also known that in acid environments the carbonate precipitations ($CaCO_3$ and $FeCO_3$) are severely increased because of the high CO_2 concentration environments.

However, the need of controlling the scaling process is due to three other major difficulties: (1) the clogging of wells and pipes, (2) the decrease in the efficiency of pumps, heat exchangers and turbines, and (3) the freezing of valves, which renders these components inoperative.[15]

2.9. Reasons for avoiding mineral deposits in geothermal plants pipelines

As already mentioned, despite a potential aid in corrosion protection, most of the depositions need to be avoided. These deposits can cause more or less serious consequences on installations, from loss of performance to the complete failure of an entire part.

2.9.1. Clogging of wells and pipes

In pipelines, scale deposits lead to a reduction in the fluid flow section and can sometimes even completely obstruct the pipeline. This phenomenon increases pressure drops and therefore more energy is needed in the pumps to maintain good fluid circulation. Scale deposits can also end up representing considerable masses, causing a significant overload to the support structures, which can cause the rupture of pipes due to the extra load.

2.9.2. Decreased thermal efficiency

Calcium carbonate, for example, has a very low thermal conductivity when compared to metals (while $CaCO_3$ has an average value of 5,52 W/m.K, for different types of carbon steel this value increases to around 50 W/m.K). A deposit of scale on a surface through which heat transfer takes place leads to an increase in thermal resistance and therefore reduces thermal efficiency. This is the kind of problem caused in the case, for example, of mineral deposits in domestic kettles or pans.

2.9.3. Localized corrosion

Localized corrosion occurs when the corrosive phenomenon focuses the attack in a small area or in certain discrete points. The initiation of this mechanism is often linked to the rupture or instability of the passive film (stainless steel) or due to the presence of aggressive ions in the environment.

The most important and most contradictory effect that carbonate deposits can have is linked to localized corrosion. The thermal expansion coefficient of calcium carbonate is very different from that of metals. This difference can cause depositions to drop with changes in temperatures and, thus, create cavities that lead to a concentration of chemicals and cause the **crevice corrosion** phenomena. Galvanic corrosion is also possible between a scaly surface and a bare metal surface (in the case of metallic deposits).

Crevice corrosion is also an intense localized corrosion that frequently occurs in joints and other shielded areas on metal surfaces exposed to corrosive products. This type of attack is usually associated with small volumes of standing solution caused by holes, gasket surface, lap joints, surface deposits and crevices under bolts (or rivet heads) for example.

In short, it is initiated due to the high concentration of ions and the low concentration of oxygen, mainly in bad joints made of two different materials. Figure 6 shows a scheme of this situation.

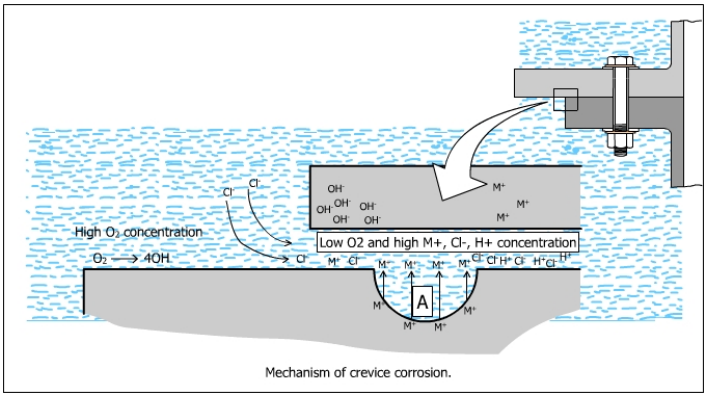

Figure 6: General scheme explaining Crevice Corrosion[20]

Regarding crevice corrosion, there are three stages: incubation, initiation and propagation. During incubation, dissolved oxygen is consumed in the occluded area. This becomes deaerated. Then, the dissolution of the passive film takes place, and after there is an electromigration of Cl- from the bulk to the occluded zone (electroneutrality) and a decrease in pH (hydrolysis of metal cations). Then, when the conditions are very aggressive, and the material can no longer repassivate itself, the mechanisms are self-sustaining and propagation takes place.

2.10. Inhibitors for the scaling processes

The idea of this part is to better understand their use and the quantities necessary for mineral deposition to be prevented.

As seen before, the onset of this precipitation can occur in several ways, for example as a result of a drop in pressure, of changes in temperature, of the entry of oxygen or of corrosive processes. Many of these processes are inevitable effects during the processing of brine in a geothermal plant, so it is important to understand and try to control the scaling process in other ways.

In addition to the choice of the most appropriate material and that one which resists scaling, we can use chemical substances that can inhibit or at least delay the process. In the present work it will be tested three different inhibitors: the Ferrofos 8450 from the product line Ferrofos, the TurboDispin 4363 both of them made by Kurita and also another solution made of 1-diphosphonic acid (HEDP).

Both inhibitors are known to prevent the formation of scale from water hardness salts by blocking crystal growth (Threshold-effect). It is known that scaling inhibition through "threshold effect" treatment is the most common method that is proven to prevent or reduce mineral deposits. Threshold scale inhibitors effectively inhibit mineral scale growth at concentrations of 1000 times less than a balanced stoichiometric ratio of scaling cations. There are three main roles for these types of inhibitors.[23]

(1) Nucleation inhibition: It involves the disruption/redissolving of the growing nuclei. In this mechanism, the scaling inhibitors interact with the first growing crystals; then the inhibitor acts as a nucleation center that covers the scale formed in the aggregate. Thus, active crystal growth sites are blocked and further crystal growth is stopped.

(2) Crystal distortion: In this mechanism, it is believed that the inhibitor will interfere with the nucleation process or rate by adsorption at the active sites of the crystals and distortion of its morphology. Thus, the formation of a regular morphology and a stable crystalline lattice is prevented and the accumulation of an adherent scale is avoided

(3) Dispersion or Anti-Agglomeration: In this mechanism, the negatively charged parts of an inhibitor adsorb onto scale micro-crystals. In so, they generate relatively high ionic charges that separate the particles and prevent them from agglomerating and settling as suspended particles. This prevents the crystal from adhering to a surface and growing into a scale deposit (i.e. ionic particles are kept suspended in solution).

2.10.1. HEDP

One of the main and best-known scale inhibitors nowadays in the market is the HEDP, abbreviation for *Hydroxyethylidene Diphosphonic Acid*. HEDP is an organic phosphonic acid scale inhibitor. It can form a stable complex with metal ions such as iron, copper, and zinc. HEDP can remove and reduce the quantity of metal ions dissolved in water. HEDP can dissolve the oxide on the metal surface.[26]

HEDP has an excellent chelating capacity (ability to fix metal ions, forming a chelate complex that is soluble) for certain metal cations such as Ca^{2+}, Mg^{2+}, Cu^{2+}, Zn^{2+} and the like. This water treatment agent also has a fouling inhibition effect by distortion of the crystalline network and solubilization of the complexes formed.

HEDP has known fouling inhibition and corrosion inhibition functions. The fouling inhibition effect can be achieved using only a small dose of the product (Threshold effect). They are the most widely used corrosion and scale inhibitors in the treatment of circulating cooling water, for example. Its fouling inhibition performance is excellent, particularly important at low temperatures (below 250°C).[26]

For these temperature values, the product could already be used in most geothermal salt pans, but the product is still proven effective even at higher temperatures, despite a slightly lower performance.

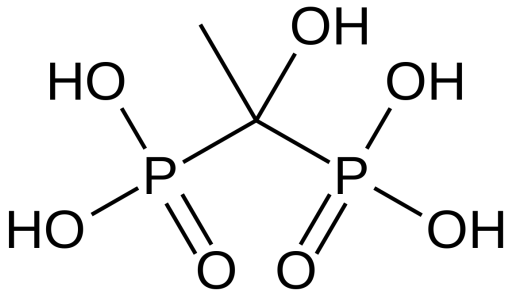

Figure 7: HEDP Structure Scheme

2.10.2. Ferrofos 8450 (Kurita) and TurboDispin 4363 (Kurita)

The products are part of a big and known family of products made by Kurita. Both product lines have a wide range of scaling and corrosion inhibitors offered by the enterprise. Those products were mainly designed to prevent corrosion of steel, copper and copper alloys by formation of a protective layer on the surface.

As all the ferrofos products, it is a blend of phosphonic acids and organic polymers in water.[24] According to *M. Mpelwa* and *S. Tang* [23] for this type of composition, the most important inhibiting effects are linked to the mechanism of nucleation inhibition (although the three mechanisms happen at the same time). In fact, it promotes the formation of a protective layer to limit corrosion of steel, copper and its alloys.

It is worth mentioning that among other products present in the Ferrofos 8450, as in any product of the Ferrofos family, there is always a phosphonic acid acting as an important product for its scaling inhibiting properties.

2.11. Main Goals of This Work

As shown earlier during the presentation of the bibliographic base, mineral depositions that frequently occur on the pipeline metallic surfaces of geothermal plants are highly undesirable.

The main goal of the experimental part of this work is to better understand the mechanisms of mineral deposition (mainly of calcium carbonate) on carbon steel surfaces and also how to prevent this process from occurring with the aid of inhibitors. The main idea is to reach optimal concentrations for the use of each inhibitor.

To obtain this knowledge, several methods were used, which will be explained.

3. Techniques and Experimental Conditions

3.1. Electrolyte Composition

At the beginning, it was used as a "corrosive environment", the kind of water with the highest concentration of mineral salts that is sold in France (Hepar is the brand of water), the idea was to create an electrolyte that represents well the geothermal fluids and it worked. But after some tests the idea of using a less loaded water (Volvic) emerged, to compare their scaling power and scaling time. In the table 4 below, we can analyze its composition.

The first electrolyte used, Hepar commercial water, was chosen for its high content of Ca^{2+} ions. A major advantage of using commercial water is the consistency of its chemical composition. Despite reaching good concentrations of Sulfates, Bicarbonates and Calcium for the experiments, it was not possible, with this solution, to simulate the different pHs of the geothermal fluids.

Afterwards a much less charged water was used (Volvic) in order to compare the scaling power of the solutions and to show the important role that the electrolyte has during electrochemical experiments.

Table 4 : Hepar and Volvic Waters Compositions (mg/L)

Water Type	Calcium (Ca)	Magnesium (Mg)	Bicarbonates	Sodium (Na)	Sulfates (SO_4^{2-})	Nitrates (NO_3^-)	Fluor (F)	Chlorures (Cl^-)	Average pH
Hepar	549,0	119,0	383,7	14,2	1530,0	4,3	0,40	18,8	7.4
Volvic	11,5	8,0	71,0	11,6	8,1	6,3	0,22	13,5	7.0

Note: For the Hepar water, the data was sent by the company while the data from Volvic was obtained from the bottle label

3.2. Choice of the Steel Samples

Analyzing the annexed table 2, it is possible to note the similarities in the carbon content between the most used carbon steel in geothermal power plants and the carbon steels XC38 and XC42, and they were also the two that we followed in most of the carried out experiments. It is possible to compare them respectively to the API N80 and to the API P110 sorts. Some tests with stainless steel 316L were done aiming to compare their properties and results.

3.3. Experimental Setup for testing accelerated scaling

The experimental procedure has already been reproduced in similar ways by a student from 5SGM 2019/2020. The idea of this project is to continue the measurements started by him and to improve the experimental protocols. As seen in the scheme and picture shown in figure 8, the experimental assembly used is a common 3-electrodes assembly associated with a double-walled electrochemical cell with a volume of 80 mL.

Basically, it consists of a rotating disk electrode (carbon or stainless steel), a silver chloride (Ag/AgCl - 3M KCl with sat. AgCl) reference electrode and a platinum cylinder grid electrode as a counter electrode. The three electrodes are connected to a potentiostat (BioLogic VSP) that is driven by a software called EC-Lab.

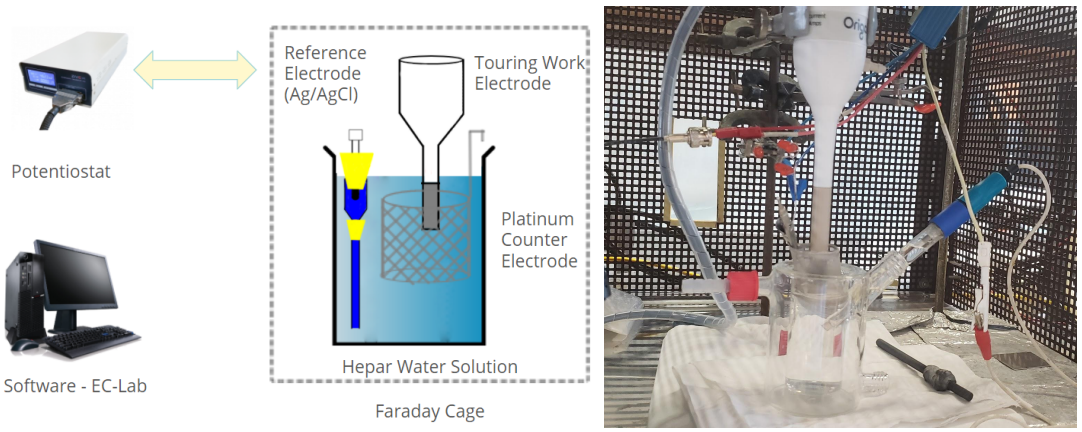

Figure 8: Schematic and Picture of the experimental setup

The idea of this apparatus is to enable the simulation of environments close to those found in geothermal fields, so that we can test the various responses of the steels used, for example the levels of mineral deposits, the potential for corrosion etc.

3.3.1. Working Electrode

The working electrodes used in this research project were manufactured at INSA's mechanical workshop (Atelier Mécanique). There were samples made in carbon steel (XC38 and XC42) and in stainless steel (316L) in two different forms: 40mm cylinder samples and 5mm disc-shaped samples (detailed schematic drawn in the annexed figure 1). These last ones were asked for analysis purposes (fits inside the microscope (SEM) and X-Ray diffractogram for example). According to the study made the year before, it was possible to set an optimal rotation speed of 300 rpm for every experiment.

These cylindrical electrodes are only intended for electrochemical analysis (potentiodynamic curves, chronoamperometry and electrochemical impedance spectroscopy measurements) meanwhile the rotating disk-shaped electrodes were also used for chemical analysis. In both cases they are covered by a heat shrinkable tubing so that only one disk-shaped face is in contact with the electrolyte (as shown in figure 9). The surface of the disk is 1 cm^2 and the other end has a thread to fix the electrode in the rotating device.

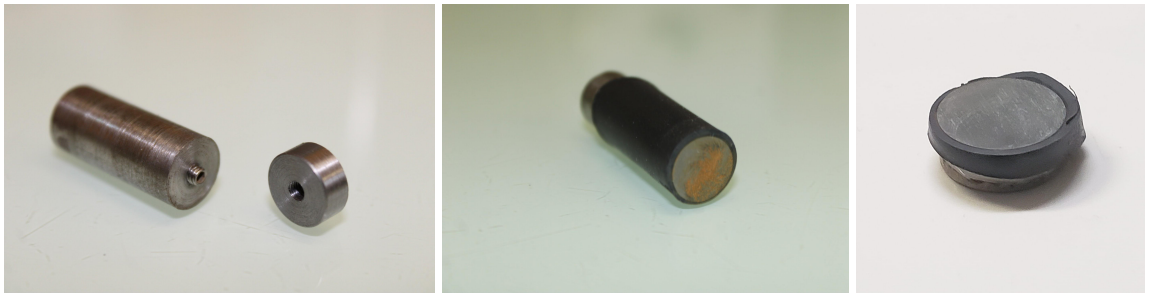

Figure 9: Photos of the Working Electrodes

3.3.2. Reference Electrode

The reference electrode used is a silver chloride (Ag/AgCl) electrode E11.OGL.014 (3M KCl with sat. AgCl). It has a rigorously constant and reproducible potential located at 0.197 V in relation to the normal hydrogen electrode. Its potential is fixed by the redox balance between the metallic silver Ag and the ions Ag^+ whose concentration is fixed by the solubility of the silver chloride AgCl.

The reference electrode is placed as close as possible to the working electrode in order to limit measurement errors due to the ohmic drop induced by imperfections with the electrolyte.

3.3.3. Counter Electrode

The counter electrode used is a fine tubular mesh made of platinum. Its function is to guarantee the passage of the electric current in the set of three electrodes, minimizing the effect of polarization and ohmic drop in the vicinity of the working electrode. The tubular shape allows uniform conditions on the surface of the working electrode. Its dimensions are sufficient to not limit the reaction that occurs at the working electrode.

3.4. Sample preparation

3.4.1. Heating Shrinkable Tubing

The first step of the preparation is the adherence of the rubber around the cylinders. But before being heated with the hot air thermal blower the samples went through a stringent cleaning sequence with ethanol, acetone and a thermal ultrasonic bath. After the heating process, it is important to verify that the entire internal surface of the rubber is well attached to the surface of the steel and that all the glue has been thermally activated. The equipment used during the process are shown in figure 10.

Figure 10: Thermal Ultrasonic Bath (left) | Hot Air Thermal Blower (center) | Heat Shrinkable Tubing application (right)

3.4.2. Polishing methods

Before every experiment, the sample went through very methodical polishing steps. The polishing discs sequence used (P180, P320, P600, P1200) is shown in figure 11. With the proviso that, for the flattened samples (with 5mm), the polishing process must be done very carefully, to prevent the useful surface from being overly polished and reaching the screw hole as shown in the annexed figures 2 and 3.

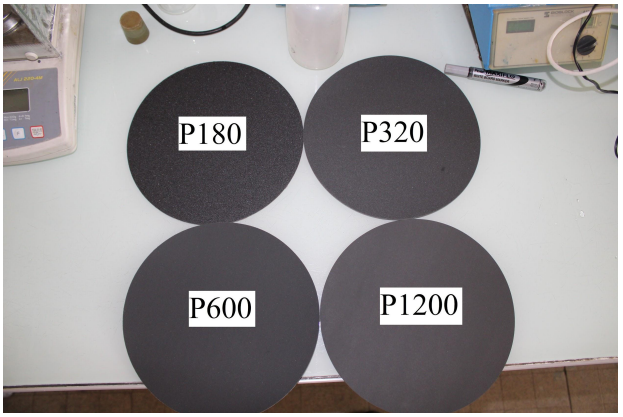

Figure 11: Polishing Discs Sequence used.

3.5. Electrochemical Techniques

This part of the study is dedicated to the explanation of the physico-chemical techniques used in the experiments.

3.5.1. Polarization Curves

A polarization curve is obtained by linearly scanning a predefined range of potentials while measuring the current intensity. Thus, it is possible to obtain information about the interactions that occur in the studied environment, such as the reduction of water or oxygen or the oxidation of the metal and also to have kinetic data of the corrosion process.

To perform this test, it is necessary to consider several influencing parameters, because any reaction involving electrons will have an impact on the polarization curve and on the metal surface state itself. It is necessary, then, to take into account the nature of the metal electrode and the electrolyte, the scanning speed of the potential, the temperature, the flow of electrolyte current, since all the above parameters have some type of influence on the shape of the potential intensity curve.

It is worth remembering that it is necessary to repeat the cathodic curve test every time the experimental conditions change (nature of the electrode, temperature and/or rotation speed of the working electrode).

It can be plotted in two different ways, the first and most common way is the relative voltage in the x axis while the logarithmic scale of the current density in the y axis. However, there is another not so common way of analyzing this data, without the logarithmic scale. Those analyses are most used for understanding the passive layer formation and the pitting corrosion for stainless steel. As they are not very common, the next part is dedicated to better explain it.

3.5.1.1. Expected Round Trip Polarization Curves for Stainless Steels

Generally, it is used to analyze the relation of the material-medium pair with respect to the corrosion potential and the onset of pitting corrosion. This potential for pitting measures how resistant the material is. We can also define the protection potential, that is the potential below which there is no spread of pre-existing pits nor initiation of new ones.

These two potentials are determined experimentally by plotting a polarization curve called the roundtrip polarization curve (Figure 12). When these two potentials are practically identical, it means that the material is generally not sensitive to pitting corrosion in the considered medium.

The pitting potential depends on many factors, the main ones being the chloride content and the pH of the medium, for example.

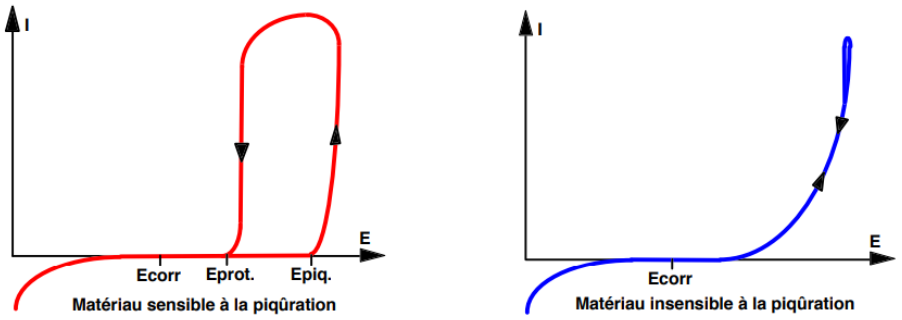

Figure 12: Examples of RoundTrip Polarization Curves for Steels[20]

Stainless steels can be classified as more or less sensitive to pitting corrosion. When the polarization return curve makes a hysteresis, it can be said that the material is sensitive to pitting corrosion, on the other hand, the closer the return curve approaches the outward curve, the more the material resists this type of corrosion.

In the case of a steel sensitive to this kind of corrosion, if the anodic potential corresponding to the depassivation of the alloy is reached, this will result in the continuation of the attack initiated, until the potential is not reduced to the protection range of the passive film. Accidental breakage of the protective film, creating an active metallic zone, can therefore lead to the appearance of localized corrosion.

For materials resistant to pitting corrosion, the attack stops as soon as the active potential is removed. In case of accidental breakage of the passive protective film, it will tend to rebuild itself after corrosion and consumption of a minimum amount of the metallic material.

The pitting corrosion is one of the main reasons (along with its price) why stainless steels are not very much used in geothermal power plants tubulation. Some experiments were made, showing the susceptibility of stainless steels to pitting corrosion even for a small concentration of chlorides (annexed figure 4).

The results of another carried out experiment are arranged in the annexed figure 4 also shows that each time the concentration of Cl^- is reduced, the corrosion becomes more unfavorable and the range of potentials where the steel can be subjected widens. This result is in agreement with expected, since adsorption of Cl^- anions on the passive film of 316L stainless steel is one of the reasons for the development of these pitting. However, even at low concentrations, the pitting corrosion may occur.

For comparison effect, a test without any presence of Cl^- was made, where it was obtained as a result an increasing line, showing the linear proportionality between the potential and the current (Ohm's law U = R.I). So, since even with a solution with 50 ppm of Cl^- ions this linear behavior was not observed, we can say that the threshold concentration of Cl^- ions is less than 50 ppm.

3.5.2. Cathodic Polarization (Chronoamperometry)

In this kind of chronoamperometry test, a constant potential is applied and the current flow is measured. This current flow is proportional to the flow of oxygen moving by convective diffusion towards the electrode, it decreases whereas the active surface is progressively blocked by the growth of the not-conductive mineral deposits.

With it, it is possible to analyze the time for which the current flow becomes small enough not to cause corrosion, this time is called "scaling time" (t_s) as shown in the figure 13 below. Actually the theoretical scaling time is calculated with the extrapolation of the main drop in current intensity. The analysis of this scaling time can lead us to understand interesting properties, as well as the scaling power of the electrolyte, the scaling resistance of a material or even the action of scaling inhibitors.

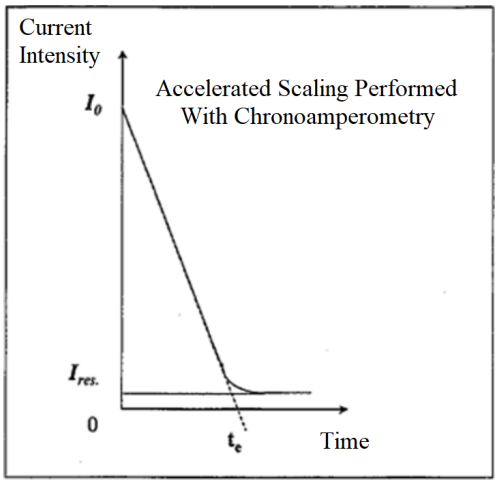

Figure 13: Example of Accelerated Scaling with Chronoamperometry

The intensity of the current that passes through the electrode decreases with time, until it reaches a practically constant value. As explained above, the decrease in current is due to the decrease in the electrode's active surface, this happens because $CaCO_3$ crystals are deposited on the surface. Meanwhile the residual current i_{res} is somewhat related to the deposit morphology, for example, the more compact and insulating the scale, the lower the residual current will be.

3.5.3. Impedance Spectroscopy (EIS)

Dielectric spectroscopy is a subcategory of many existing impedance spectroscopy techniques. With it, it is possible to measure dielectric properties of a medium as a function of frequency. The technique is based on the interaction of an external field with the electric dipole moment of the sample, often expressed by permittivity.

But for our case, its importance is linked to the characterization of electrochemical systems. This technique measures the impedance of a system in a frequency range, being able to calculate characteristics such as energy storage and dissipation properties. Frequently, the data obtained by electrochemical impedance spectroscopy (EIS) are expressed graphically in a Bode or a Nyquist graph. In the case of this work, the frequency range for all tests were between 10 mHz and 10 kHz.

Nowadays, it is relatively simple to plot those diagrams once most modern potentiostats have an impedance analyzer coupled. This pair of components allows the user to determine the charge transfer resistance, double layer capacitance and ohmic resistance.

Nyquist diagrams are made up of one or several arcs according to the complexity of the redox reactions. But we will always analyze the first two arcs, which are linked to the real values of the electrochemical reactions present here.

An impedance spectrum (Nyquist diagram) of a purely resistive material will have zero imaginary electrical impedance (Figure 14a). Otherwise, a purely capacitive material will present a spectrum typical of Figure 14b and if a material has resistive and capacitive properties it will present a typical spectrum of electrical impedance, shown in Figure 14c.

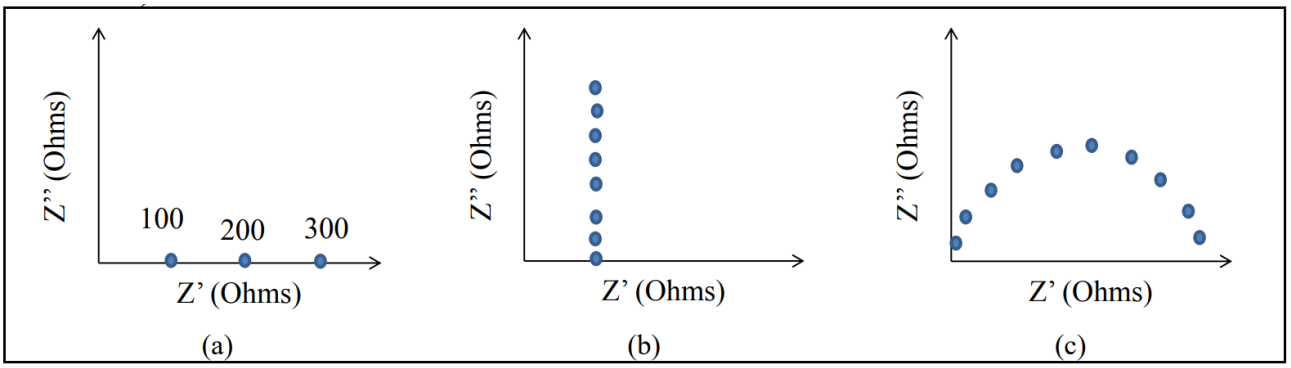

Figure 14: Example of Generic Impedance Spectrums[221]

Analyzing the example of impedance spectrum presented in the figure 15, it is possible to calculate or determine some interesting properties as well as the electrolyte resistance (R_0) and the charge transfer resistance of the sample (R_2).

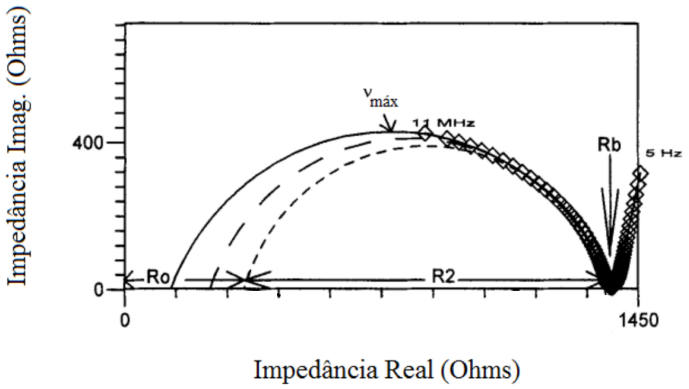

Figure 15: Real Example of Impedance Spectrum to Identify the Main Parameters[22]

3.6. Surface Analysis Techniques

3.6.1. Scanning Electron Microscopy (SEM)

As is known, the scanning electron microscope (SEM) is a type of electron microscope that produces images of a scanned surface with a focused electron beam. In the most common SEM mode, secondary electrons emitted by atoms excited by the primary electron beam are detected using a secondary electron detector (Everhart-Thornley detector). The signal strength depends, among other things, on the topography of the samples.

3.6.2. X-Ray Diffraction (XRD)

The x-ray diffraction is a technique that relies on the interaction of electromagnetic radiation with matter in crystalline form so that the structures of the crystallized molecules can be determined.

It is possible, by measuring the diffracted beams at different angles, to produce a three-dimensional image of the density of electrons within the crystal. From this electron density, the average positions of the atoms in the crystal can be determined, as well as the density of their chemical bonds, their crystallographic disorder, their crystalline structure, etc.

In short, the X-ray diffraction technique used in this work makes it possible to determine the arrangement of the atoms structure that constitute the mineral deposit on the surface.

In the case of this work, the measurements were performed with a BRUKER AXS D8 ADVANCE diffractometer, equipped with a linear detector and using a copper antatode (wavelength of K copper lines 1.54Å). The 2theta domain was defined between 20° and 90°.

4. Characterization Results and Discussion

4.1. Optimization of Polarization Curves and Scaling Time

4.1.1. Polarization Curve

The idea of plotting the polarization curves in our study is to better understand the behavior of the alloy when certain potentials are applied to it. More precisely, there are two important values to be determined with those curves: (1) the optimal potential range for performing the accelerated scaling and (2) the corrosion potential.

As the reduction of dissolved oxygen is central to the accelerated scaling method, an important point to be determined with this type of curve is the most adequate potential to perform the accelerated scaling. This optimal potential corresponds to the potential range where the dissolved oxygen reduction reaction predominates and the reduction of water is poorly developed. In the polarization curve, this interval is represented by a plateau in the cathodic domain where the current remains practically constant.

During this interval, the current corresponds only to the process limited by the diffusion of the reactive species and the charge transfer is no longer important. Analyzing the figures 16 and 17 it was possible to determine those values.

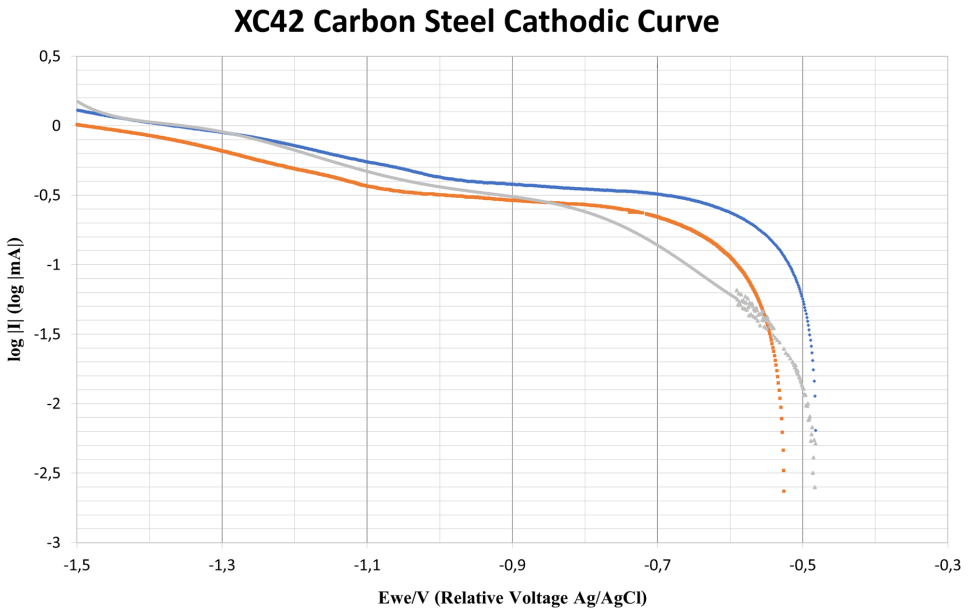

Figure 16: XC42 Carbon Steel Cathodic Curves
Scan speed: 5 mV/s

Table 5: Average Results Analyzing XC42 Carbon Steel Cathodic Curves

Results Carbon Steel XC 42	
Average of Corrosion Potential Values	- 0,509 V (Ag/AgCl)
Average of Optimal Potential for Scaling	- 0,900 V (Ag/AgCl)

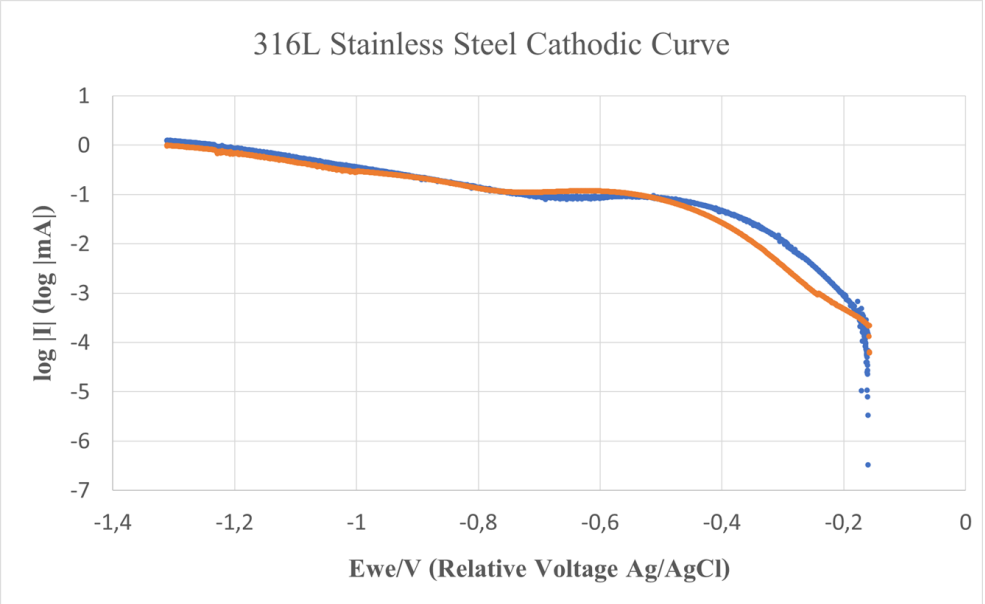

Figure 17: 316L Stainless Steel Cathodic Curves
Scan speed: 5 mV/s

Table 6: Average Results Analyzing 316L Stainless Steel Cathodic Curves

Results Stainless Steel 316L	
Average of Corrosion Potential Values	- 0,159 V (Ag/AgCl)
Average of Optimal Potential for Scaling	- 0,700 V (Ag/AgCl)

4.1.2. Scaling Time

After obtaining an optimal potential value to perform the Accelerated Scaling tests for each sample, it was possible to carry out the first series of chronoamperometry experiments. These experiments were performed aiming at the better understanding of the scaling time for each double sample-electrolyte.

Analyzing the figures 18 and 19 and using the extrapolation laws explained in the theoretical part of this report, it was possible to determine an expected scaling time (t_s) value for each case.

As shown in the article by *R Menzari et al*[27], an accelerated scaling with a similar solution resulted in scaling times around half an hour for carbon steel samples. In our case, the results were about 40 minutes for carbon steel and 5 hours and 30 minutes for stainless steel. This time difference is probably due to the passive and, therefore, much less reactive character of the stainless steel surface.

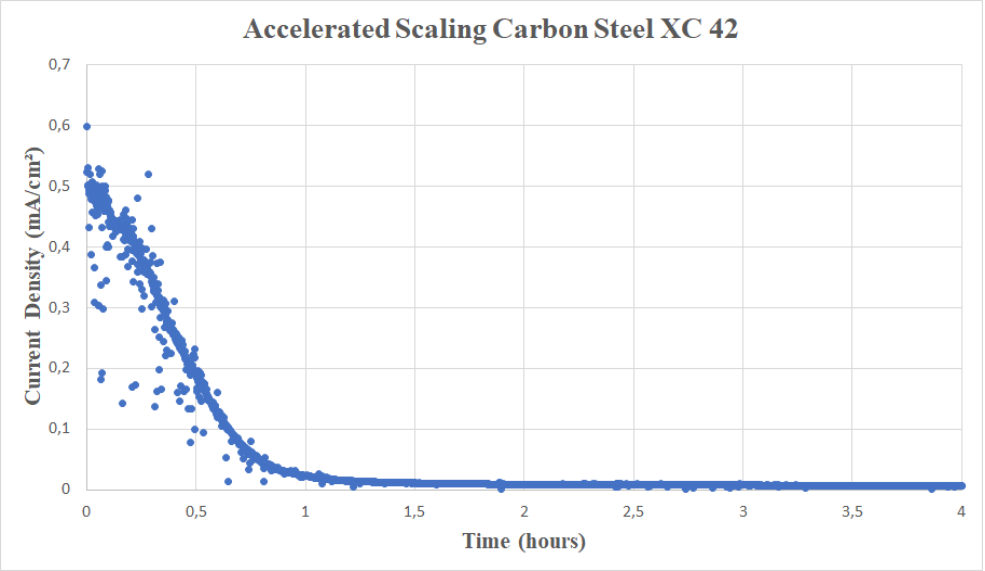

Figure 18: First series of chronoamperometry experiments for XC42 Carbon Steel (-0,9 $V_{Ag/AgCl}$) in Hepar Water

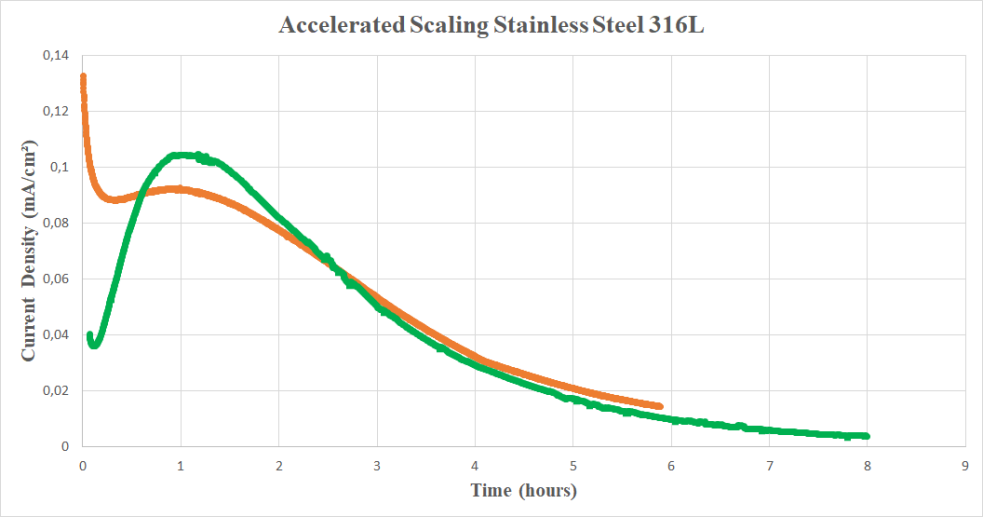

Figure 19: First series of chronoamperometry experiments for 316L Stainless Steel (-0,7 $V_{Ag/AgCl}$) in Hepar Water

Table 7: Average Scaling Time For XC42 and 316L Steels.

Average Scaling Time Without Inhibitor	
Carbon Steel XC 42	42 minutes
Stainless Steel 316L	5 hours 35 minutes

4.2. Comparative of Water Solutions

One important step of this work was the choice of the solution that would be used as electrolyte. It was known that it should contain a great amount of calcium ions to enable mineral deposition.

In addition to the high concentration of Ca^{+} ions, the choice of using commercial water was also closely linked to the facilitation of the process, as it would not be necessary to prepare electrolytic solutions for each experiment, avoiding mistakes.

This comparative study was performed only to show the importance of the electrolyte chosen in the tests. In the tests carried out with Volvic water, there was practically no decrease in the current intensity during the first hour and a half of chronoamperometry with XC42 carbon steel (Figure 20), while with 316L stainless steel the beginning of its current lowering was only after more than 3 hours (annexed figure 5).

Those results show that the scaling power of the electrolyte has a big role in those kinds of experiments.

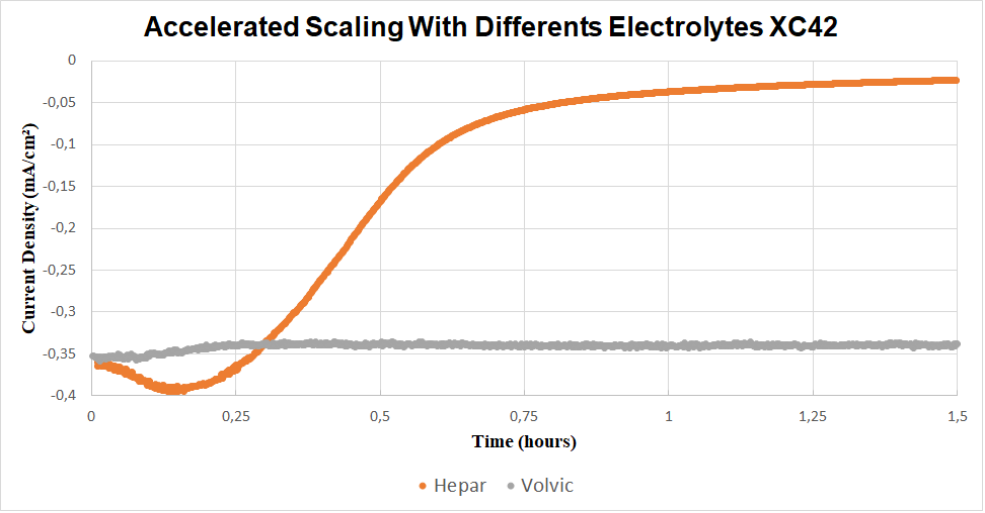

Figure 20: Accelerated Scaling of Carbon Steel XC42 samples performed with differents electrolytes (-0,9 $V_{Ag/AgCl}$)

4.3. Accelerated Scaling With or Without Inhibitors - Carbon Steel XC 42

4.3.1. Comparative Curves

After mastering the experimental techniques and protocols of the experiments, it was decided that trials with inhibitors would be started.

Due to the short period of time remaining due to the delays caused by the COVID-19 pandemic, we decided to focus our studies on carbon steel samples, leaving aside the continuity of experiments with stainless steel (although initial experiments were also carried out). This decision was made for several reasons, among them: (1) the excessive time that each experiment takes (up to eight hours for stainless steel) and (2) the greater use of carbon steel in the field of geothermal energy generation (the reasons for which have been explained previously).

As we can see in the figure 21, both types of inhibitors are effective. The effectiveness is perceived, at first, by the not-lowering of the current intensity during chronoamperometry. Analyzing the graph, it is possible to notice that in two tests carried out without the addition of inhibitors, the current reaches an almost zero value (around 0,05 mA/cm²) in less than an hour (scaling time).

However, for tests performed with the addition of inhibitors, the current intensity remains almost constant throughout the test and does not fall to values close to zero. Some variations can be caused by instability or small mineral deposits on the surface.

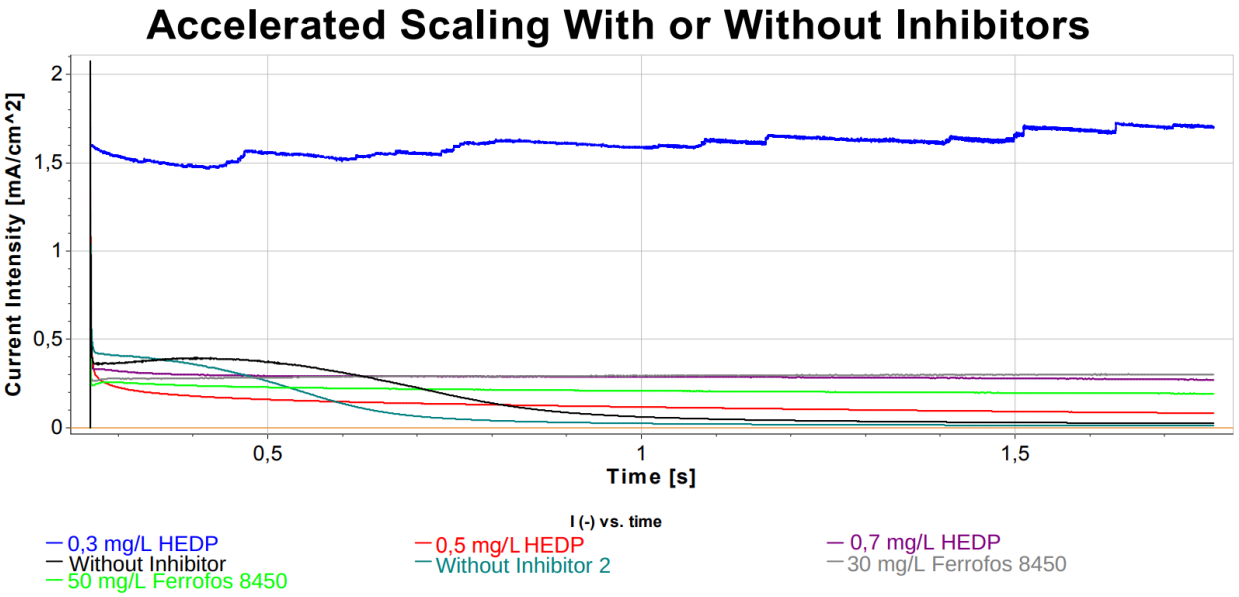

Figure 21: Comparative Accelerated Scaling Curves - With or Without Inhibitors

Table 8: Current Intensity After Stabilization

Average Current Intensity After Stabilization			
0,3 mg/L HEDP	1,67 mA/cm²	Without Inhibitor	0,05 mA/cm²
0,5 mg/L HEDP	0,18 mA/cm²	Without Inhibitor II	0,03 mA/cm²
0,7 mg/L HEDP	0,31 mA/cm²	30 mg/L Ferrofos 8450	0,33 mA/cm²
0,7 mg/L HEDP Sol II **	0,32 mA/cm²	50 mg/L Ferrofos 8450	0,24 mA/cm²
10 mg/L TurboDispin 4364**		0,31 mA/cm²	

(**) - Samples were made after and the resulting graphics are on the annexed figure 6

It is important to mention that the tests were performed at least twice to guarantee the results. An interesting point to highlight about the graphics is related to the tests with 0,3 mg/L of HEDP. In those experiments, the current intensity ended up not reaching an exactly stable point, but similar results were obtained for three different tests in which the values remained around 1.5 mA/cm² after more than one hour of chronoamperometry.

The reason why the value kept so high is unknown but it probably happened due to the presence of an unwanted conductive agent in 0,3 mg/L HEDP solution, which increased electrolyte conductivity. But the principle of comparative analysis remains the same, there is no accelerated scaling even for this inhibitor concentration.

Another hypothesis is that the amount of HEDP present in the 0,3 mg/L solution, despite avoiding the unwanted mineral deposition, is insufficient to fully cover the steel surface, inducing a higher cathodic current density.

4.4. Chemical analyzes

4.4.1. X-Ray Diffraction

In our study, a subcategory technique called X-ray powder diffraction was used. It is most widely used for the identification of unknown crystalline materials (e.g. minerals, inorganic compounds).

The most widespread use of this technique is in the identification and characterization of crystalline solids, each of which produces a distinctive diffraction pattern.

Both the positions (corresponding to lattice spacings) and the relative intensity of the lines in a diffraction pattern are indicative of a particular phase and material, providing a "fingerprint" of the crystalline structure, and with it is possible to identify different crystalline phases. A multi-phase mixture will show more than one pattern superposed, allowing for determination of the relative concentrations of phases in the mixture.

Those fingerprints will allow the identification, for example, of calcium carbonate crystals present in the samples. The measurements were performed with a BRUKER AXS D8 ADVANCE diffractometer, equipped with a linear detector and using a copper antatode (wavelength of K copper lines 1.54Å). The 2theta domain was defined between 20° and 90°. The resulting diffractograms are shown in the next figures:

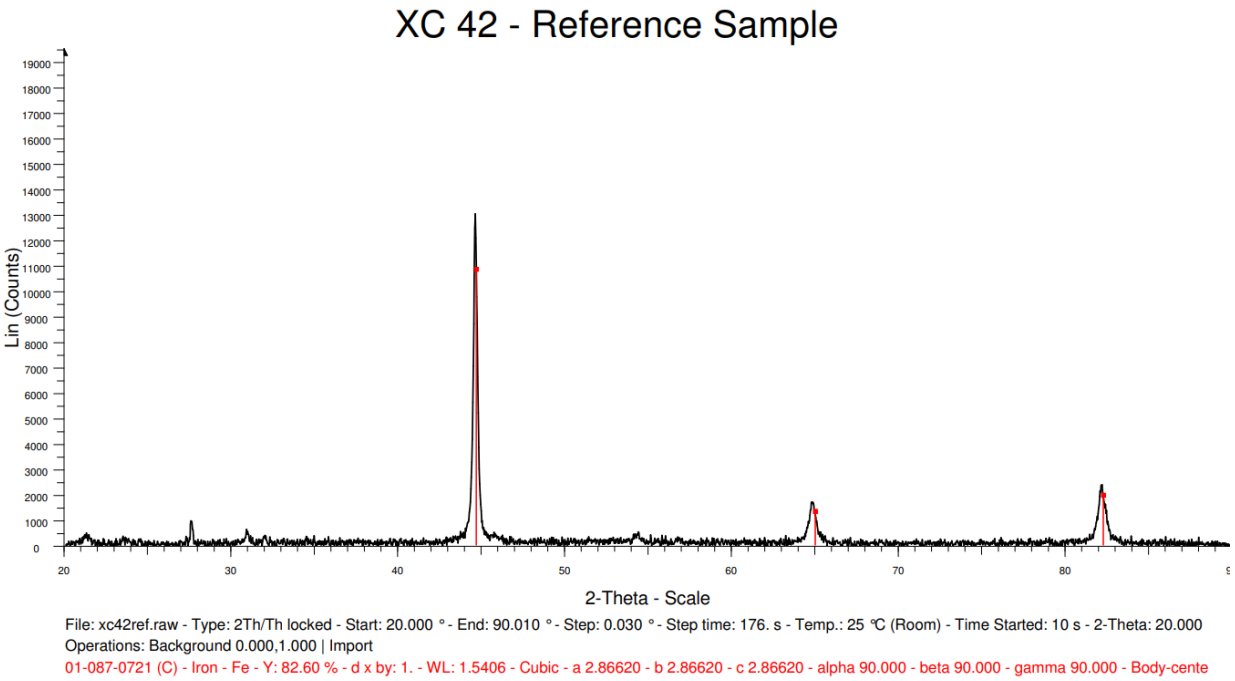

Figure 22: Results of the X-Ray Analysis - Reference Carbon Steel XC 42 Sample

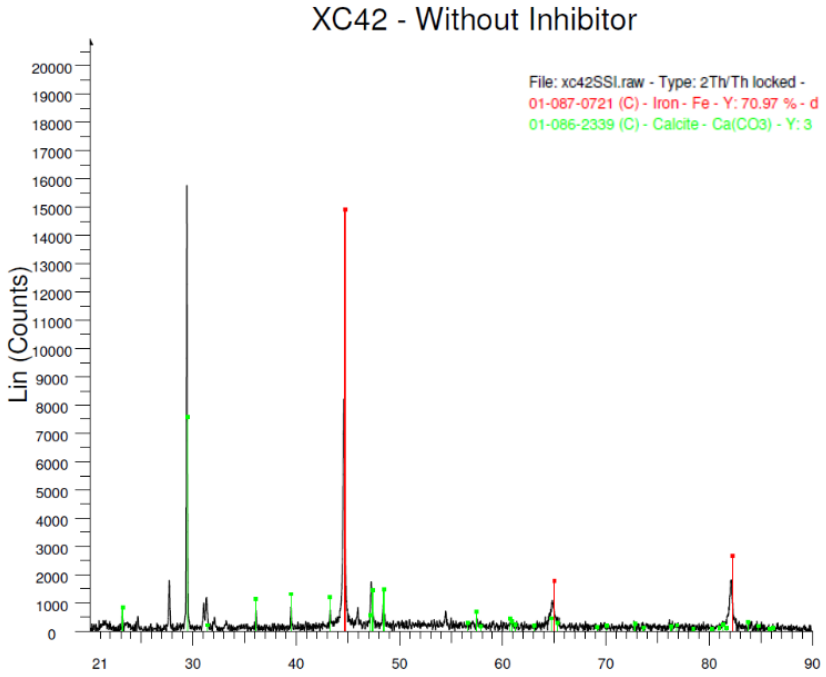

Figure 23: Results of the X-Ray Analysis - Carbon Steel XC42 Experiment Without Inhibitor

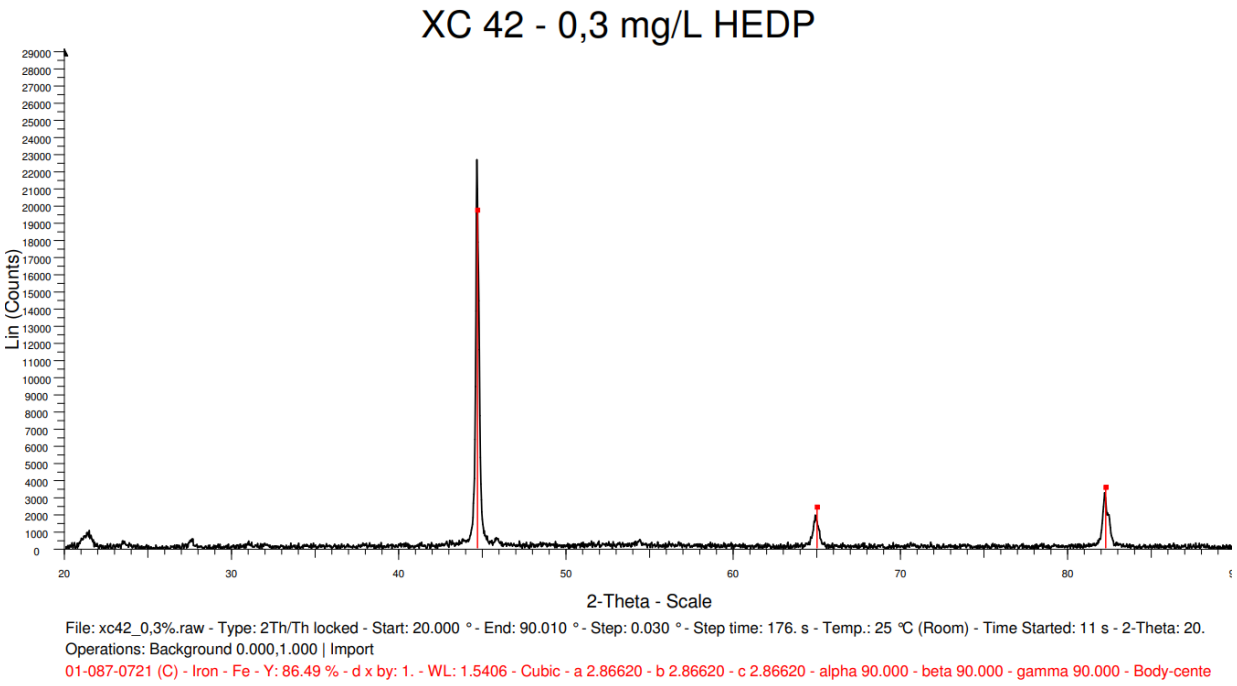

Figure 24: Results of the X-Ray Analysis - Carbon Steel XC 42 Experiment With 0,3 mg/L HEDP

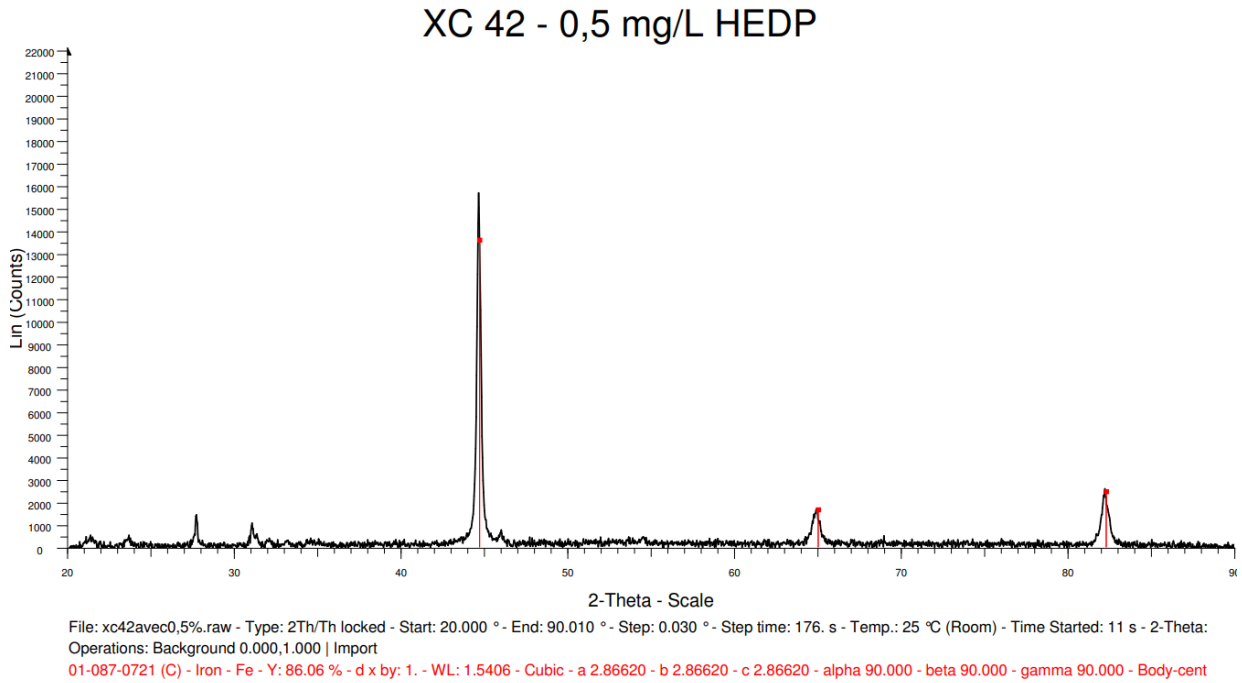

Figure 25: Results of the X-Ray Analysis - Carbon Steel XC 42 Experiment With 0,5 mg/L HEDP

There are other studies in the literature that show similar results for X Ray Diffraction spectra of mineral deposition from geothermal brines, even in brines with different compositions. The article written by *J. Pauwels et al* have results that also show the formation of Halite (a Sodium Chloride mineral aglomerate),[32] in addition to the calcite and aragonite that were also obtained in this experiment.

Performing such an experiment on the samples that went through the Accelerated Scaling process, it was possible to compare if there were or not a considerable amount of mineral deposits on the surface. Analyzing the figures 21 to 25, it is noted that there are not great differences between the reference sample and the ones with 0,3 mg/L and 0,5 mg/L HEDP Inhibitors, meanwhile the $CaCO_3$ peaks are clearly visible in the results of the experiments without inhibitors.

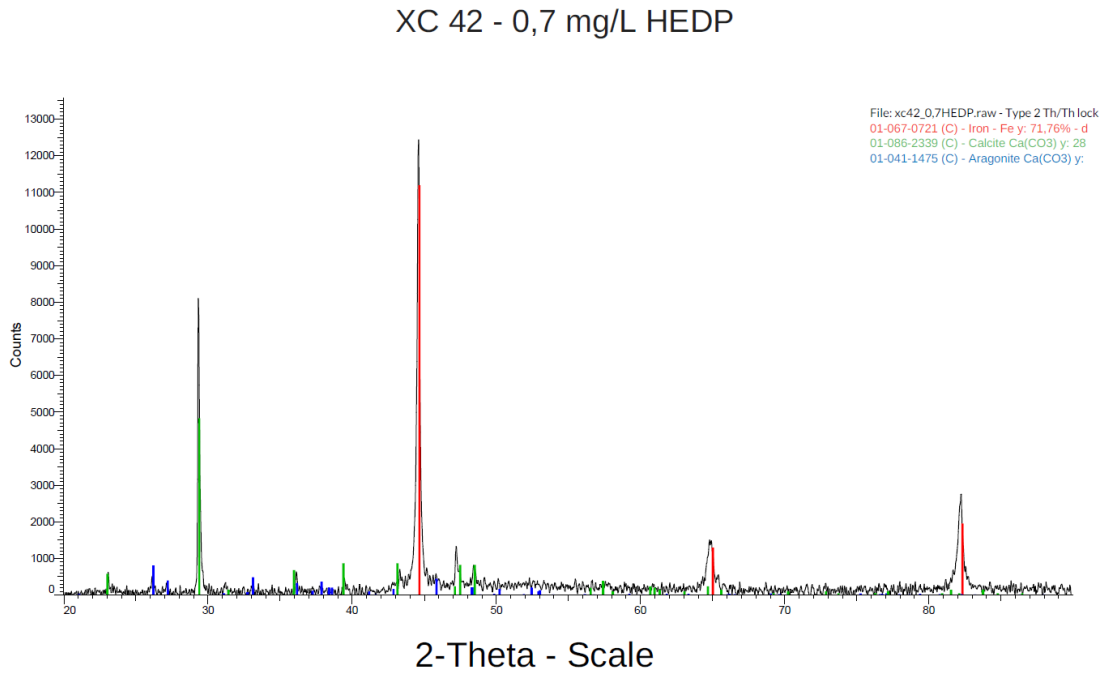

Figure 26: Results of the X-Ray Analysis - Carbon Steel XC 42 Experiment With 0,7 mg/L HEDP

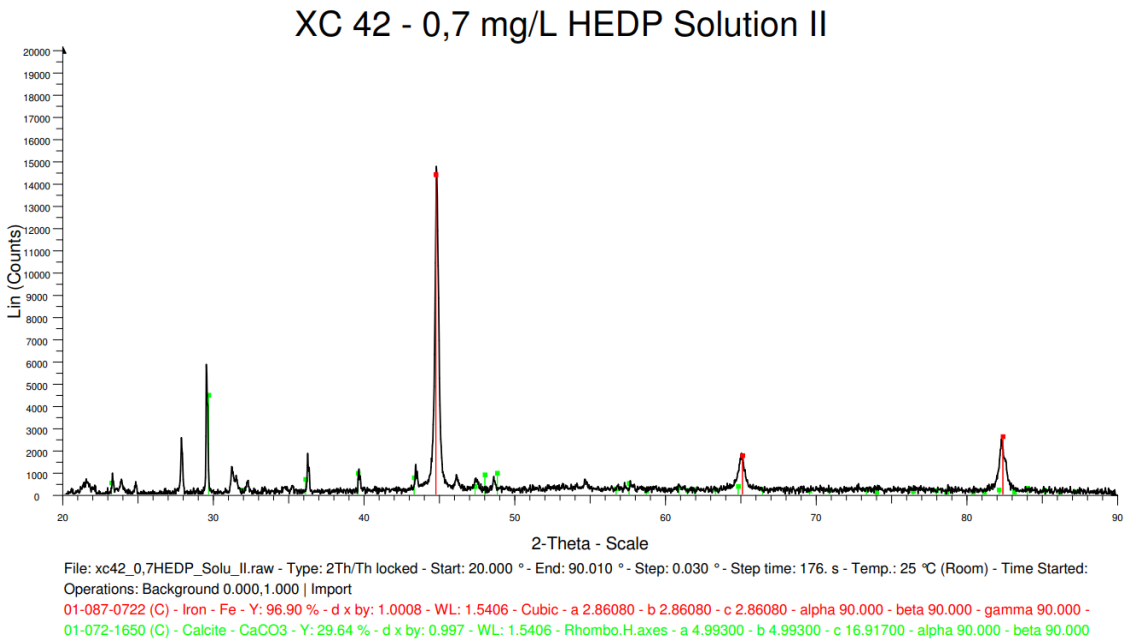

Figure 27: Results of the X-Ray Analysis - Carbon Steel XC 42 Experiment With 0,7 mg/L HEDP Solution II

However, for the experiment made with 0,7 mg/L (figures 26 and 27) it was possible to see a considerable calcium carbonate peak, although less intense than the experiment without inhibitors. In addition, it is worth mentioning the appearance of a small peak of Aragonite, another possible morphology of deposition of the calcium carbonate crystals. It is possible that the excess of HEDP interferes with the formation of the crystals of Calcite, which can cause changes in its final morphology.

With 0,3 and 0,5 mg/L concentrations, HEDP: (1) completely avoid the growing of the mineral deposits, (2) were adsorbed on the surface, preventing the fixation of mineral deposits on it and/or (3) the amount of mineral deposited on the surface was not enough to be detected in X-Ray Diffraction.

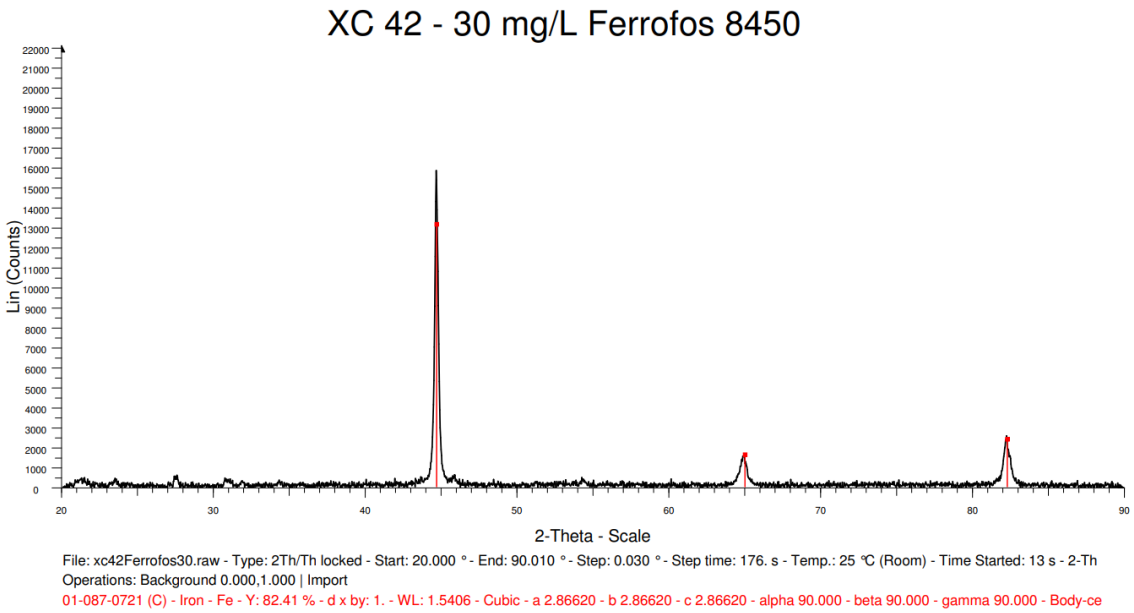

Figure 28: Results of the X-Ray Analysis - Carbon Steel XC 42 Experiment With 30 mg/L Ferrofos 8450

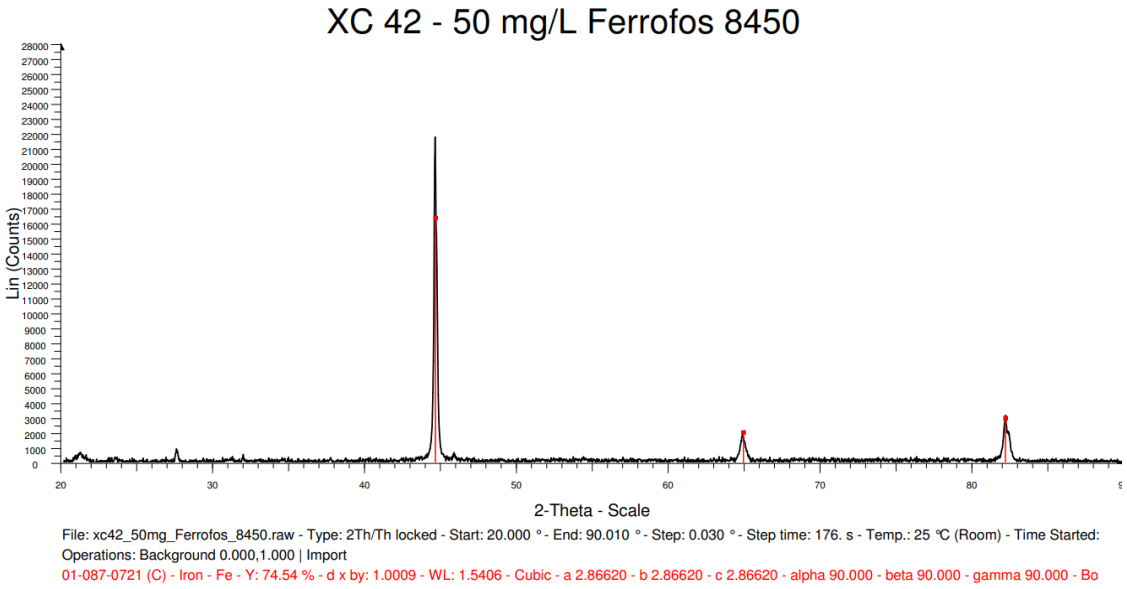

Figure 29: Results of the X-Ray Analysis - Carbon Steel XC 42 Experiment With 50 mg/L Ferrofos 8450

While analyzing the results for the second inhibitor used, it is clear that Ferrofos 8450 has been shown to have a great potential for prevention against the scaling process of calcium carbonate on a metallic surface. The differences between the difratograms present in figures 28 and 29 have no significant differences and, therefore, an optimum concentration of better performance cannot be guaranteed just with this characterization test.

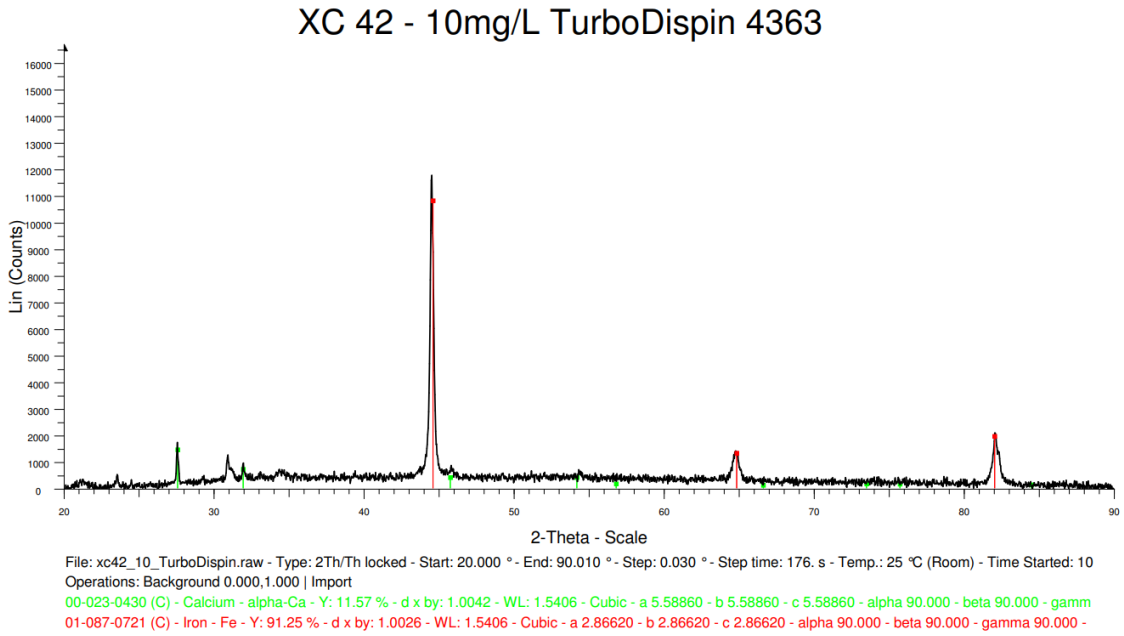

Figure 30: Results of the X-Ray Analysis - Carbon Steel XC 42 Experiment With 10 mg/L TurboDispin 4363

However, the last tested inhibitor (TurboDIspin 4363), despite having a potential efficiency, showed that when used at 10 mg/L it does not completely prevent mineral deposits from appearing. The peaks of calcium-containing materials shown in figure 30 are much less intense than those found in samples that were subjected to tests without inhibitors, so it is expected that when in higher concentrations, the product will be able to prevent mineral formations from happening.

4.4.2. Scanning Electron Microscopy Images

The Tescan Vega3 scanning electron microscope, located on the first floor of the Blaise Pascal building (Sciences et Génie des Matériaux INSA Lyon) was used to characterize the surface of the metal samples after accelerated scaling.

In the case of samples whose surface is covered by a deposit of $CaCO_3$, the acquisition of SEM good quality images could be complicated and problematic. In this case, the deposits, by their insulating nature, will store the incident electrons without being able to reflect them, which will have the effect of causing charging phenomena to appear on the images.

To try to overcome this problem, it is preferable to use a low beam intensity and a fast scan speed. For obtaining good quality images, it is also possible to use the media acquisition mode, which allows you to average a large number of images obtained at high scanning speed, which allows to avoid excessively large charging phenomena and helps to obtain a clear image.

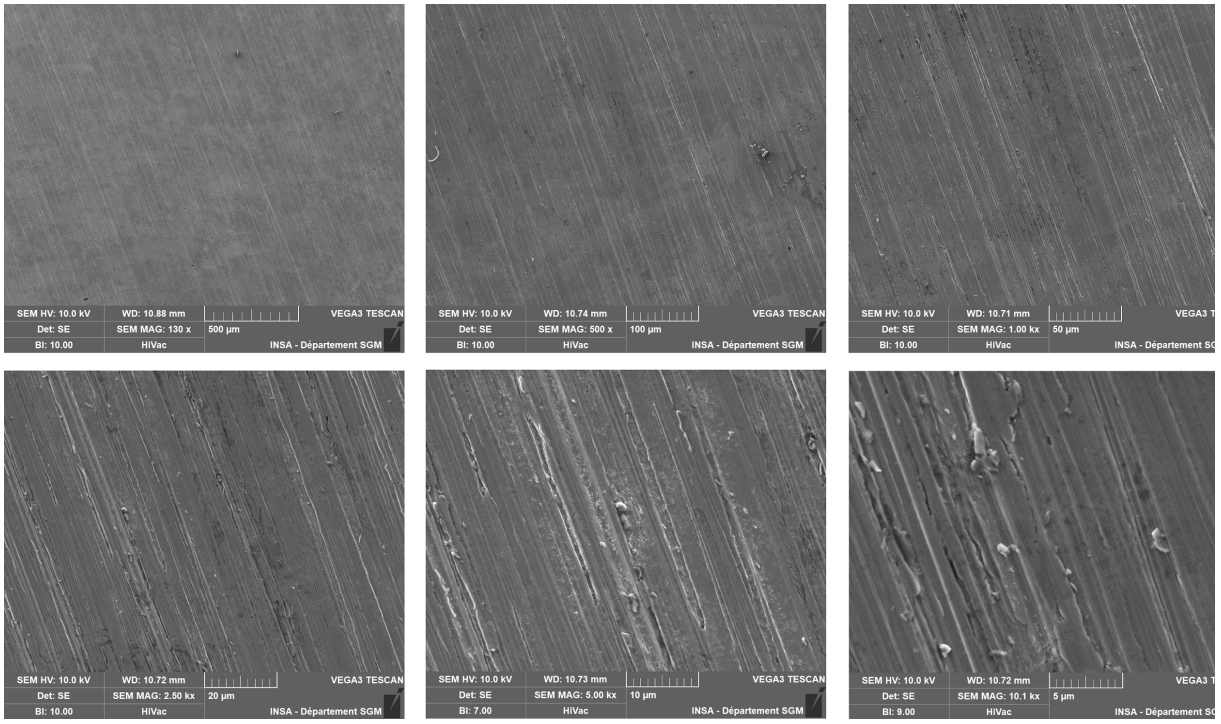

Figure 31: SEM Images - Carbon Steel Reference Sample

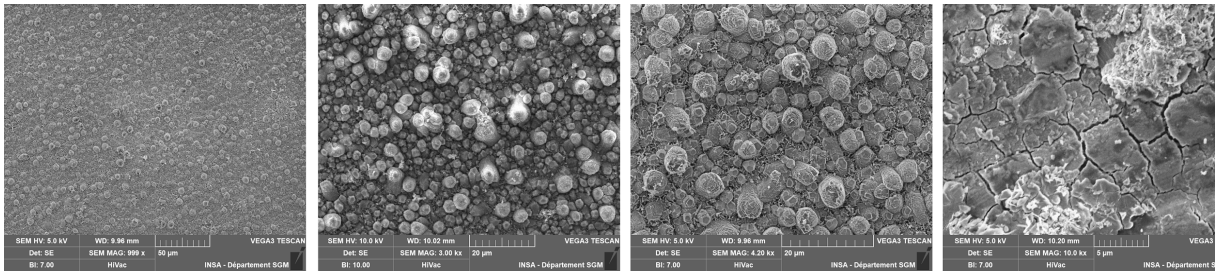

Figure 32: SEM Images - Carbon Steel Sample Without Inhibitor - Experiment I

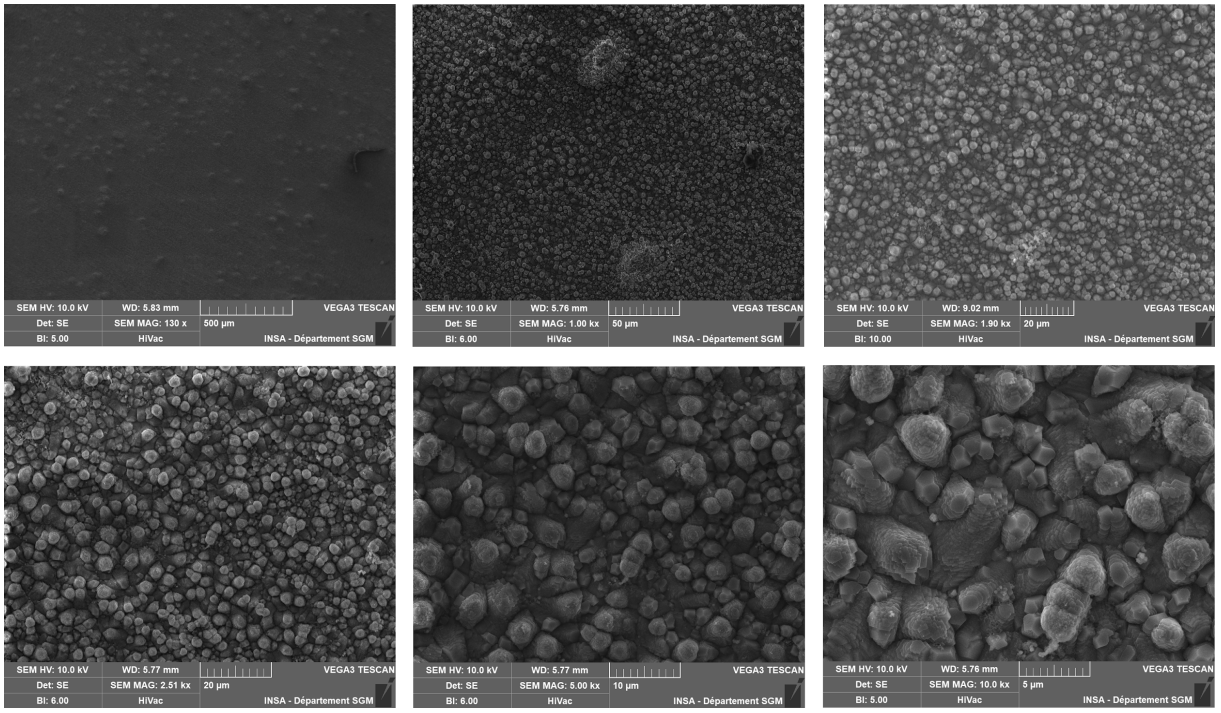

Figure 33: SEM Images - Carbon Steel Sample Without Inhibitor - Experiment II

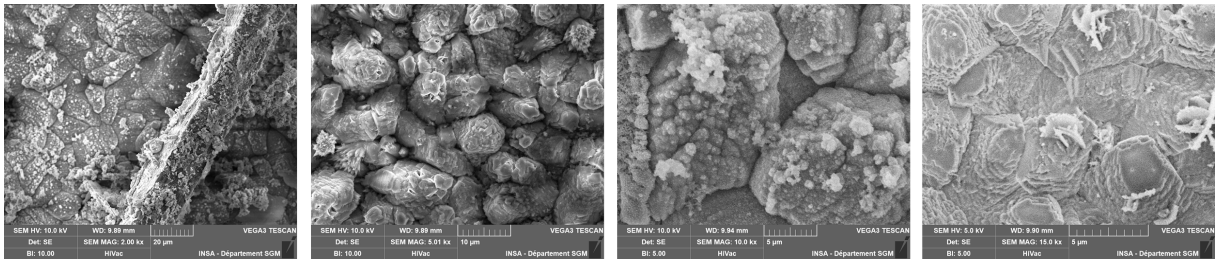

Figure 34: SEM Images - Carbon Steel Sample Without Inhibitor - $CaCO_3$ Morphology Details (Old XC38 sample)
The sample was left for 5 hours in one of the first chronoamperometric tests performed in this work.

Analyzing the images of samples that went through accelerated scaling chronoamperometry tests it is possible to see the difference between them and a reference sample that did not go through any experiment. The $CaCO_3$ crystals present on the surface of the samples without inhibitors are very characteristic and can be easily identified on a metallic surface.

On the samples without any inhibitor, it is possible to observe a dense layer of $CaCO_3$ on the surface, very similar to other mineral deposition images found in literature.[29][30] When compared to the reference one, there is clearly a difference of morphology between the surfaces. This corroborates the results seen in the analysis of x-ray diffractograms, showing a great and intense peak of calcium carbonate.

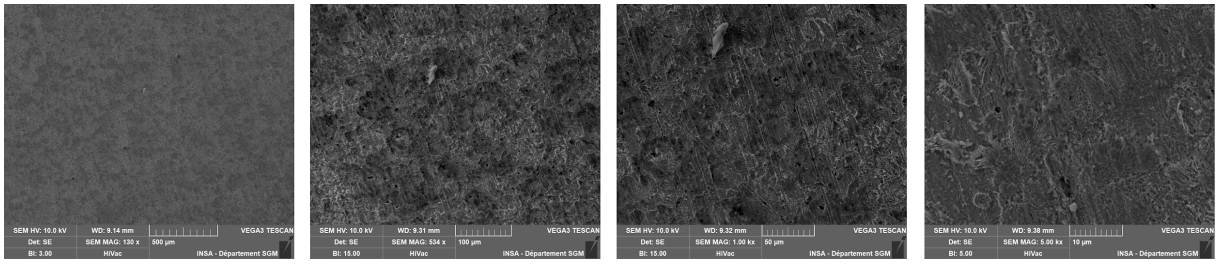

Figure 35: SEM Images - Carbon Steel Sample 0,3 mg/L HEDP - Experiment I

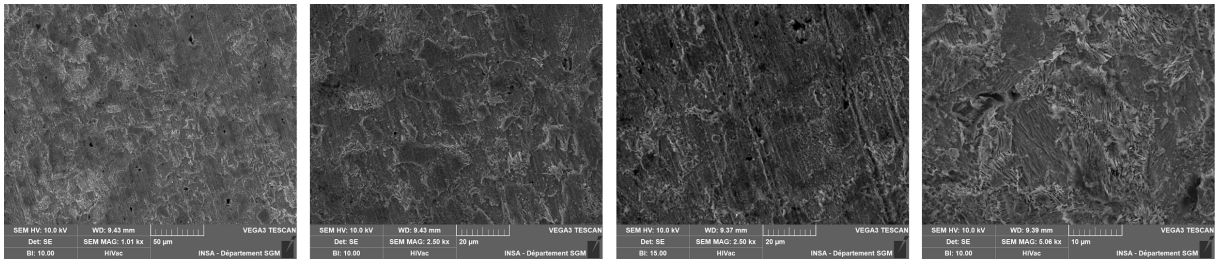

Figure 36: SEM Images - Carbon Steel Sample 0,3 mg/L HEDP - Experiment II

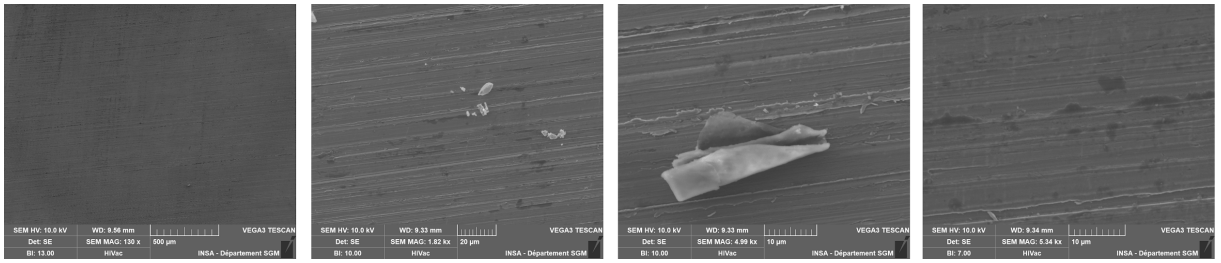

Figure 37: SEM Images - Carbon Steel Sample 0,5 mg/L HEDP - Experiment I

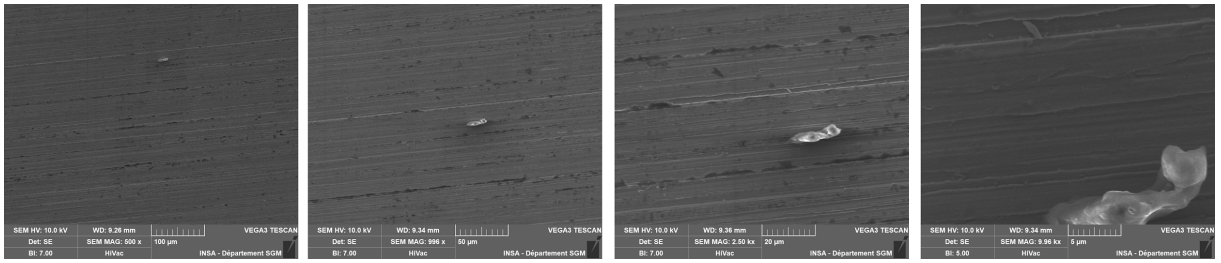

Figure 38: SEM Images - Carbon Steel Sample 0,5 mg/L HEDP - Experiment II

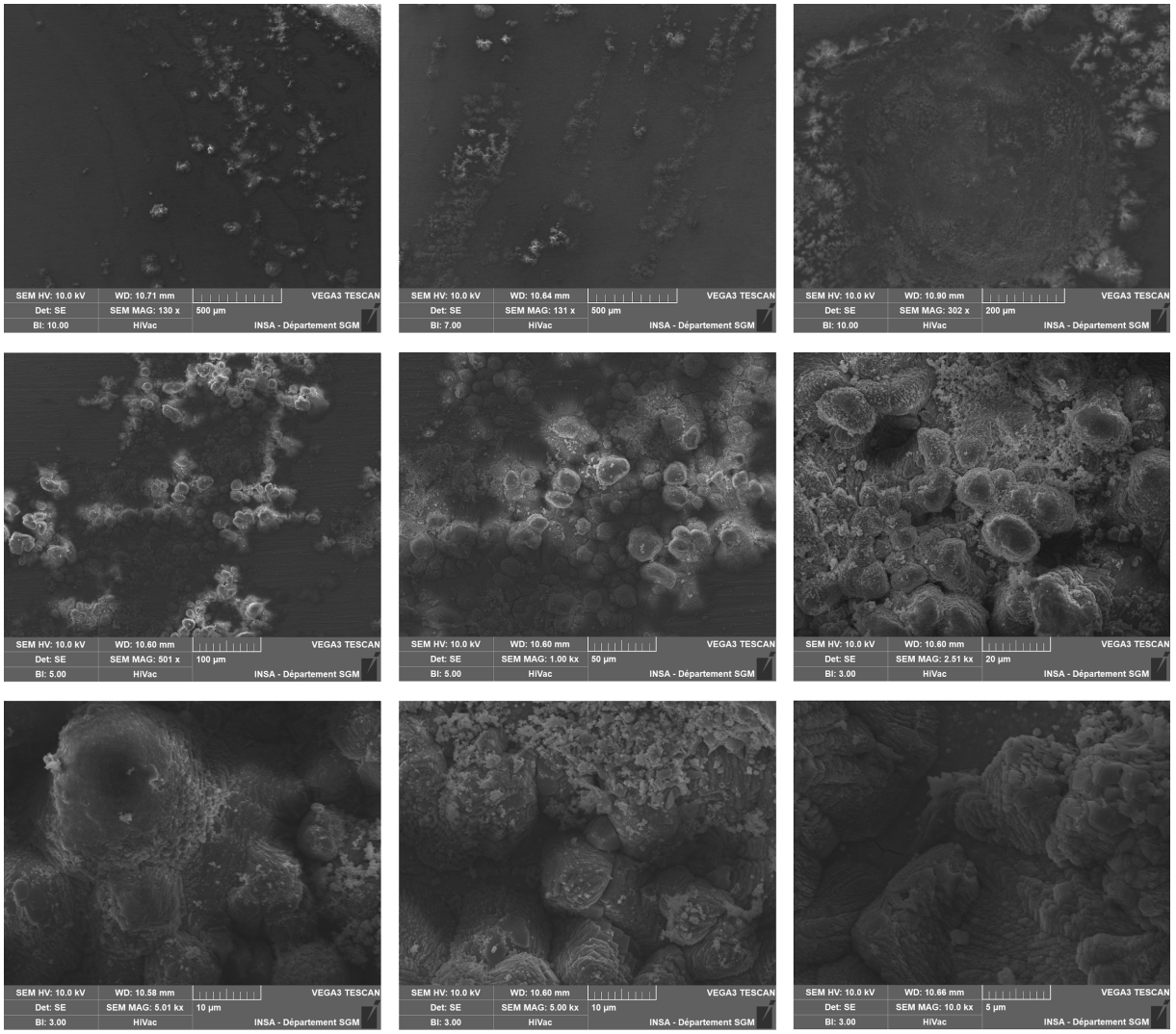

Figure 39: SEM Images - Carbon Steel Sample 0,7 mg/L HEDP - Experiment I

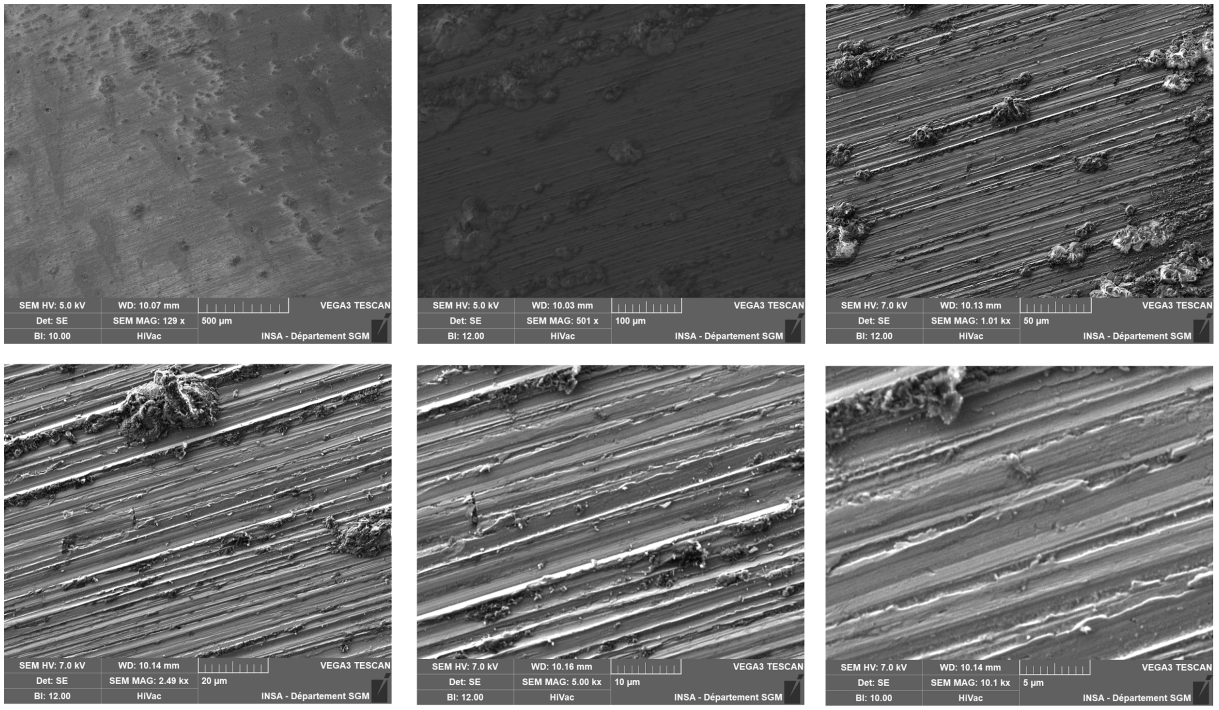

Figure 40: SEM Images - Carbon Steel Sample 0,7 mg/L HEDP Solution - Experiment II

When dealing with the images of the samples in which the HEDP inhibitor was used, it is possible to note its good effectiveness in preventing mineral deposits on the metal surface. This happens when in concentrations of 0,3 mg/L and 0,5 mg/L, however when a concentration of 0,7 mg/L was used, a certain deposition of calcium carbonate is noted, although it is much less dense and much more irregular than that presented by sample without inhibitor. This result again agrees with those obtained in the x-ray diffractograms, since the $CaCO_3$ peaks for these samples are less intense.

There are no known reasons why in the tests using the 0,7 mg/L HEDP solution some mineral deposition occurred. Perhaps this concentration is exacerbated and will hinder the inhibitory effect. Perhaps we can count on solution preparation errors, as these are very small concentrations and volumes, the separate solution to integrate the experiment may not be completely homogeneous and may contain less inhibitor.

After obtaining this unexpected result for the concentrations of 0,7 mg/L of HEDP, it was decided to prepare a new solution with the same concentration so that the set of tests was redone. Analyzing the SEM images of the samples (figure 40) whose tests were carried out with the second solution, the effectiveness of HEDP at 0,7 mg/L is even more evident, although there are still some clusters of mineral deposits on its surface.

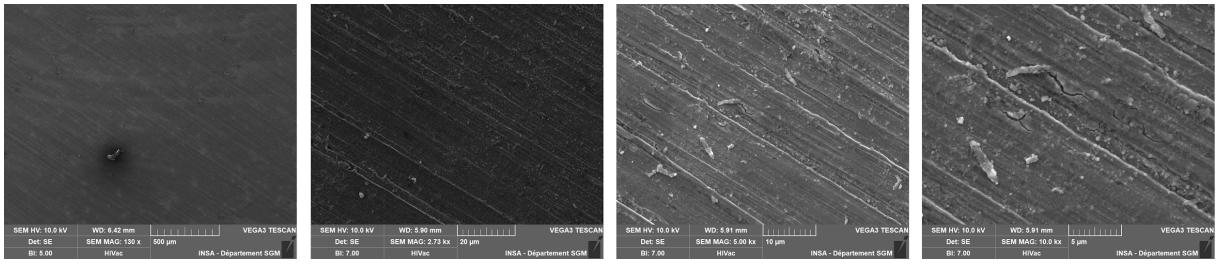

Figure 41: SEM Images - Carbon Steel Sample 30 mg/L Ferrofos 8450

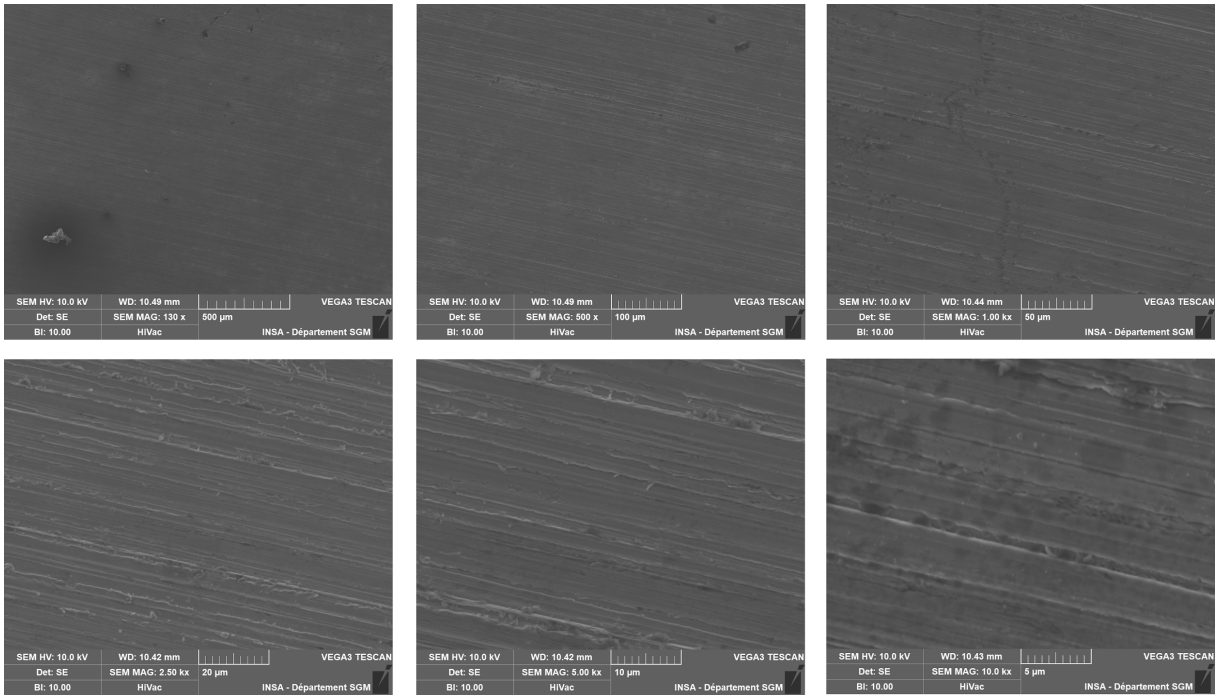

Figure 42: SEM Images - Carbon Steel Sample 50 mg/L Ferrofos 8450

Another inhibitor tested was made with the commercial corrosion and scaling inhibitor: Ferrofos 8450. The extreme similarity between the samples in which the product in question was used and the reference samples are exacerbating. Despite the small amount, it is still possible to observe a few crystals of calcium carbonate in tests with 30 mg/L of this inhibitor. Whereas in the images of the experiment at 50 mg/L, the crystals are practically nonexistent and the morphological similarities with the reference sample are even greater.

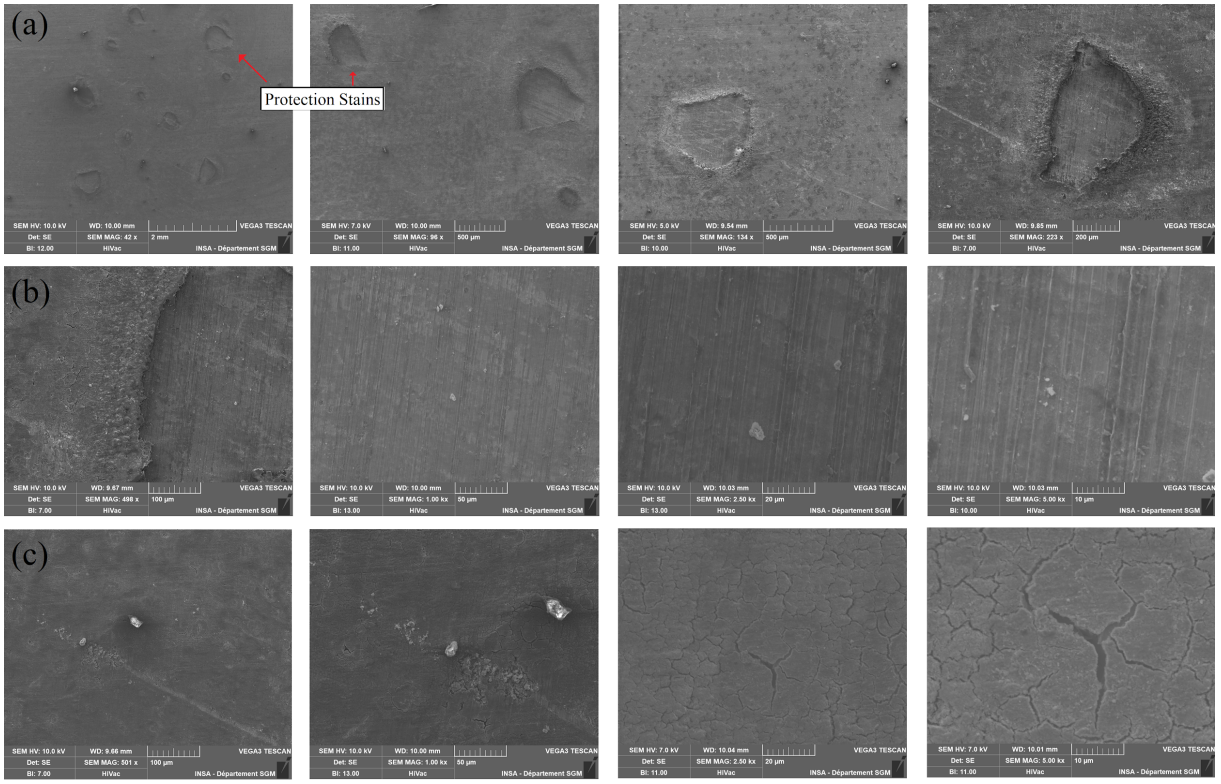

Figure 43: SEM Images - Carbon Steel Sample 10 mg/L TurboDispin 4363

The last inhibitor studied was the TurboDispin 4363. For this product the results are quite interesting. It is possible to note stains on the sample surface, analyzing it with SEM it was noted that inside that stains (figure 43 lines *a* and *b*) the surface is pretty much unchanged, concluding that there was neither mineral deposition nor corrosion products. Analyzing outside the stains (figure 43 line *c*) there are some notable differences between this surface and the ones that had mineral deposition.

Analyzing the morphology it is possible to note just a few mineral deposition but the majority of the surface consists of cracks, probably related to the corrosion products formed. This analysis allowed us to conclude that the amount of TurboDispin 4363 used was able to stop and avoid the scaling but it must have been almost all consumed and, therefore, the hypothesis is that there was not enough product left to maintain the anti-corrosive effect.

4.4.3. Electrochemical Impedance Spectroscopy

As mentioned earlier, the impedance of a circuit generally has a real part and an imaginary part, and the graphical representation of these quantities is called an impedance spectrum. The most common representations for impedance, in the context of electrical circuits, are the Nyquist (or Argand) and Bode diagrams.

In the Nyquist diagram (complex plane), the imaginary part Z" of the impedance is represented as a function of the real part Z' for different frequency values. Thus, each point in this type of graph represents the impedance at a given frequency.

Nyquist diagrams are one of the most commonly used analyses in electrochemical literature, because they enable the prediction of circuit elements, facilitating for example the construction of an equivalent electrical model for the system (along with Bode Diagrams).

In our case, it will be used alternately between trials, for example, to evaluate and compare the effectiveness of inhibitors by studying the charge transfer resistance. The frequency range for all tests were between 10 mHz and 10 kHz.

The protocol for this experiment consisted of two impedance measurements at two moments in the experiment. The first one during the accelerated scaling process (under a constant applied voltage) and the second one after the end of the process (with no applied voltage).

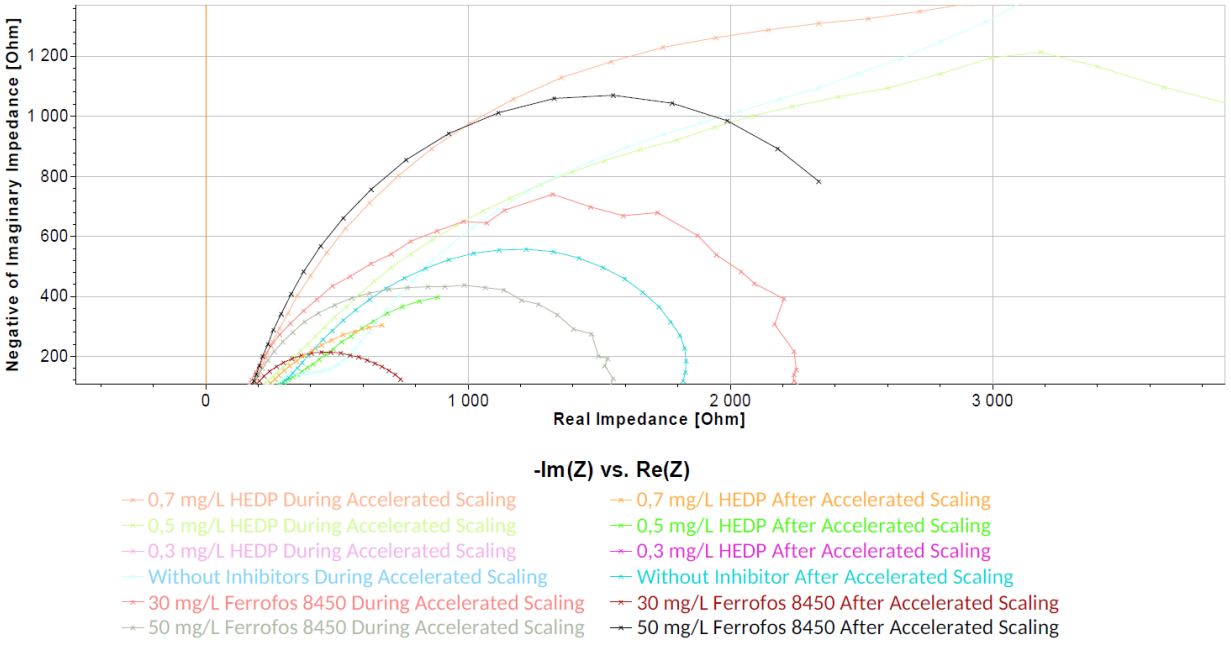

Figure 44: Nyquist Diagrams obtained from the Carbon Steel Samples - Out zoomed.

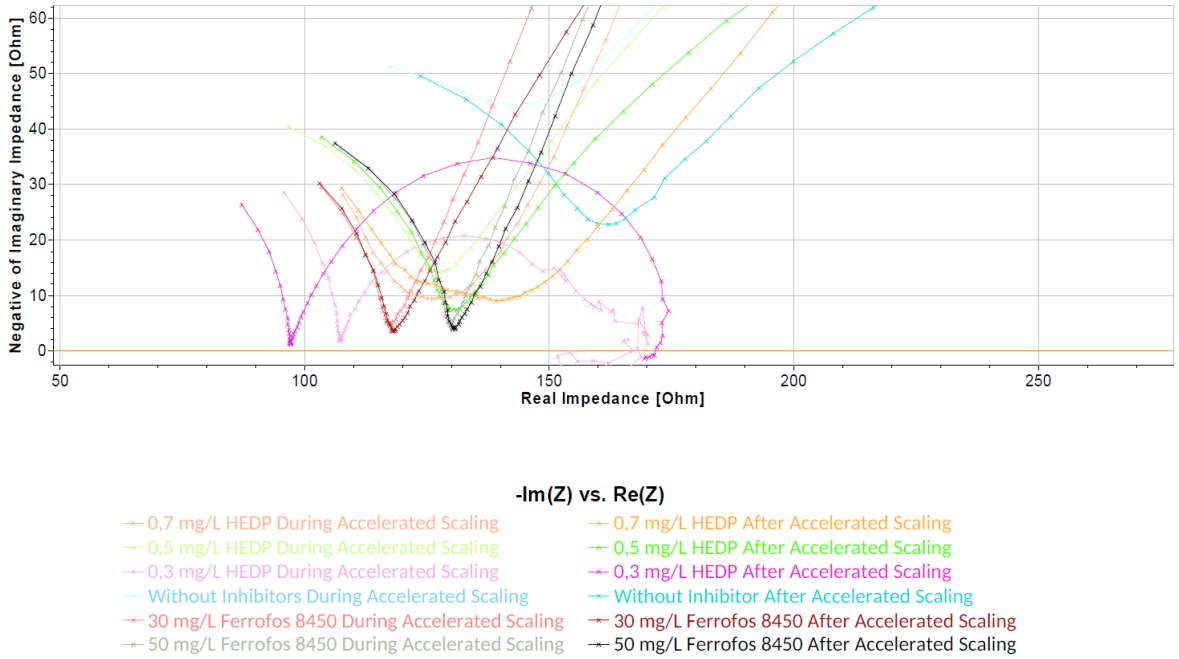

Figure 45: Nyquist Diagrams obtained from the Carbon Steel Samples - Zoomed at the beginning.

Analyzing the diagrams, Table 9 could be constructed. Of course that only looking for those results it is unlikely to conclude whether or not there was mineral deposition on the samples surface.

Table 9 : Electrical Resistance values extracted from the previous Nyquist Diagrams (XC42 Samples)

	Electrolyte Resistance (Ohm)	Sample Resistance During Scaling (Ohm)	Sample Resistance Average After Scaling (Ohm)
Without Inhibitor	154	9234 - 154 = 9080 *	1822 - 154 = 1668
0,3 mg/L HEDP	103	162 - 103 = 59	175 - 103 = 72
0,5 mg/L HEDP	129	4376 - 129 = 4247 *	1273 - 129 = 1044 *
0,7 mg/L HEDP	134	1797 - 134 = 5745 *	1050 - 134 = 916 *
0,7 mg/L HEDP Second Solution **	137	1642 - 137 = 1505	791 - 137 = 654 *
30 mg/L Ferrofos 8450	118	2217 - 118 = 2099 *	784 - 118 = 666
50 mg/L Ferrofos 8450	131	1582 - 131 = 1451	2947 - 131 = 2816 *
10 mg/L TurboDispin 4363 **	118	3341 - 118 = 3223	259 - 118 = 141

(*) - Estimated values with extrapolation of the curve
(**) - Graphic on the annexed figure 7

As shown in the Annexed Figure 1, the samples have a diameter of 11.3 mm, resulting in an area of approximately 100.29 mm². It is possible then to calculate the resistivity of the material in each case. Simply divide the value shown in table 9 by the area and the result will be the resistivity of the sample in ohm.mm².

Once the samples have an extremely complex geometry, it is difficult to calculate its exact resistivity. But as they all have the same geometry, you can use the resistance values in a comparative way.

But knowing that the calcium carbonate crystals have an extremely insulating character when compared to metallic materials, it is possible to predict that when there is mineral deposition, there will be an increase in the charge transfer resistance of the sample. Besides that, the High Frequencies arc nearly disappeared, thus giving evidence of scale removal/not-growth in the presence of the inhibitors.[25]

The results obtained from the impedance diagrams are in agreement with this theory, since the sample with the greatest charge transfer resistance during the scaling process was the one whose electrolytic solution did not contain any inhibitor type.

As previously said, it is not possible to conclude that there was mineral deposition just because the resistance increased, since other factors can influence, for example the adsorption of the inhibitor itself on the surface, if the layer is homogeneous enough, it could also be a barrier to current flow, causing the electrical resistance value to increase. Therefore, it is necessary to analyze the results as a whole to prove or not the existence of mineral deposits on the surface of the samples.

Another interesting conclusion that could be obtained is related to the corrosion rate after scaling. Those data can be earned by analyzing the intensity of the low frequency arc. In short, the corrosion rate has an inverse relationship of proportionality with the radius of the curve, i.e if the arc has a smaller radius, it means that the corrosion rate is higher for that solution-sample set.

Knowing this relation between the radius and the corrosion rate, it is possible to conclude that for 0,3 mg/L of HEDP, the corrosion rate is about 20 times higher than for experiments without inhibitors. When analyzing the curve of the tests with 0,5 mg/L HEDP, practically the same corrosion rate is observed as the experiment without inhibitors, but without scale, showing to be, apparently, the best compromise for scale inhibition and no increase of corrosion rate for HEDP.

Regarding the experiments with Ferrofos 8450, it was possible to conclude the excellent inhibitory action in the scaling process for the two concentrations used in the experiments. However, for tests with 30 mg/L, the corrosion rate after scaling was much higher than that obtained with tests without inhibitors. In the case of the tests with 50 mg/L, the corrosion rate did not increase considerably in relation to the tests without inhibitors, showing that the latter concentration is the best for the use of this inhibitor.

Unfortunately, it was not possible to obtain enough time to test other concentrations for the TurboDispin 4363 inhibitor. With a single set of experiments performed, it was possible to note that its scaling inhibitory action is quite interesting, however when used in concentrations of 10 mg/L it does not inhibit corrosion (high corrosion speed in the curve after scaling, in addition to being visually more corroded as seen in the annexed figure 8)

The fact that the higher concentrations of inhibitors also prevent the increase in the corrosion rate is probably due to two important factors, the excess of inhibitor present in the solution can: (1) continue to act in the protection against corrosion, since the three inhibitors also have corrosion inhibiting functions and/or (2) promote a protective and not-conductive layer on the steel surface, which also explains the increase in the resistivity of the sample even without observing mineral depositions.

5. Conclusions

The experiments and studies carried out in this work show that all these methods are complementary to one another, and each of them have contributed to improving our knowledge on $CaCO_3$ precipitation, scaling potential evaluation and accelerated scaling mechanisms.

Nevertheless, it is necessary to take into consideration their representativeness in relation to a real scaling phenomenon that occurs inside the pipeline of geothermal facilities. After all, an accelerated test is not always an accurate representation of a real scaling formation which may develop over several months or even over several years, and which brings into play not only the fluid's intrinsic characteristics but also complex water distribution installations and materials.

In addition, the experiments carried out in this work were performed at 30°C, not taking into account the real high temperatures of the geothermal fluids. Therefore, all the data and results presented here serve as a comparative aspect between the tests carried out, so that it is possible to have an idea of the action of mineral deposits and also of three very promising products in the treatment against mineral deposition (HEDP, Ferrofos 8450 and TurboDispin 4363).

The chronoamperometry accelerated scaling used in this work showed to be a good method to evaluate the scaling power of different fluids. With this method it was possible to induce the mineral deposits and to conclude for which tests there were (or not) significant deposits. Afterwards the presence or absence of the deposited material was proven with the aid of other analyzes: (1) SEM images, (2) X-ray diffractograms and (3) Electrochemical Impedance Spectroscopies.

With the combination of these three techniques, it was possible to prove the effectiveness of the three tested inhibitors, avoiding the growth of calcium carbonate crystals. In other words, after the tests containing the inhibitors (0,3 mg/L HEDP, 0,5 mg/L HEDP, 30 mg/L Ferrofos 8450, 50 mg/L Ferrofos 8450 and 10 mg/L TurboDispin 4363), it was not possible to identify important amounts of mineral deposits on the surface of the samples.

In addition, the results gave us indications that Ferrofos 8450 was the most effective product for the experimental conditions adopted in this work.

However, in spite of being a very promising product, there was not enough time to perform experiments with different concentrations of TurboDispin 4363, but the results indicate that with higher concentrations its anti-corrosive effect is probably sufficient to protect the metal surface (to be verified with future experiments).

Finally, it was possible to note with this study that indeed the used products have scaling inhibiting properties but its concentration in the solution plays a very important role during its effectiveness both in the scaling process and in the corrosion process..

Despite the difficulties caused by the confinement due to the pandemic and the damage caused by the SARS-Cov virus, it was possible to complete much of what was planned for this End of Study Project.

6. Bibliography

[1] ISO 8044, "*Corrosion des métaux et alliages – Termes principaux et définitions*" (2000). Accessed on 16 Oct, 2020

[2] D. Landolt, Corrosion and surface chemistry of metals (EPFL Press, Lausanne, 2007).

[3] OZGENER, L.; HEPBASLI, A.; DINCER, I. "*Parametric study of the effect of dead state on energy and energy efficiencies of geothermal district heating systems*". Heat Transfer Engineering, 2007. Accessed on 19 Oct, 2020.

[4] IRENA (International Renewable Energy Agency) - "*Renewable energy statistics 2020*". Accessed on 21 Oct, 2020.

[5] Schreiber S, Lapanje A, Ramsak P, Breembroek G. "*Operational issues in geothermal energy in Europe; status and overview*". Reykjavik (Iceland): Geothermal ERA NET; 2016. Accessed on 22/10/2020

[6] Iberl, P., Alt, N.S.A. and Schluecker, E. (2015), Evaluation of corrosion of materials for application in geothermal systems in Central Europe. Materials and Corrosion, 66: 733-755. doi: 10.1002/maco.201407864

[7] de Carvalho Albertini, José Álvaro; Susana M. Giampietri Lebrão; Mário Leite Pereira Filho. "*Estudo da Influência da Corrente Alternada na Corrosão em Dutos Metálicos Enterrados*" Artigo Mauá 2008 - Accessed on 01/03/2021

[8] Nogara, J.; Zarrouk, S. J. Corrosion in Geothermal Environment: Part 1: Fluids and Their Impact. Renewable and Sustainable Energy Reviews2018, 82, 1333–1346.

[9] Iberl, P.; Alt, N. S. A.; Schluecker, E. Evaluation of Corrosion of Materials for Application in Geothermal Systems in Central Europe: Evaluation of Corrosion of Materials in Geothermal Systems. Materials and Corrosion 2015, 66, 733–755.

[10] H. S. Klapper, R.Bäßler, J. Sobetzki, K. Weidauer, D. Stürzbecher, Materials and Corrosion. 2012, 64, 764.

[11] H. Klapper, R. Bäßler, A. Saadat, H. Asteman,Proceedings of the *NACE Conference and Expo*, NACE International, 2011.

[12] Continental Alloys database <https://www.contalloy.com/products/> Accessed on 13/01/2021

[13] "Merkblatt 821–Edelstahl Rostfrei–Eigenschaften", Informationsstelle Edelstahl Rostfrei, Düsseldorf 2012

[14] J. F. Gülich,Kreiselpumpen, Springer, Berlin Heidelberg, Heidelberg 2010

[15] N. Mundhenk, P. Huttenloch, B. Sanjuan, T. Kohl, H. Steger,R. Zorn, "*Corrosion and scaling as interrelated phenomena in an operating geothermal power plant*" - Corrosion Science 2013, Volume 70, pages 17-28.

[16] Guneysi, E. "Common Corrosion Types (Pitting and Crevice Corrosion)" .

[17] Z. Panossian.; E. W. Laurino; S. E. Abud Filho; J H de L.Oliver; N L de Almeida.; G. de S. Pimenta; M L P. Filho; J Á de C.Albertini; D de L. Silva. "*Evaluation Of Ac Corrosion In Pipelines Buried Using Ac-Probe | NACE CORROSION | OnePetro*" - NACE International, Houston, Texas, March 2011. Accessed on 20/01/2021

[18] Mundhenk, N. & Petra, Huttenloch & Scheiber, Julia & Genter, Albert & Zorn, R. & Kohl, Thomas. "*Corrosion and Scaling in the Geothermal Cycle of Soultz-sous-Forêts (France) | NACE CORROSION | OnePetro*." - NACE International, San Antonio, Texas, March 2014. Accessed on 20/01/2021

[19] Composition database: HUNAN Standard Steel: <Casing Pipe, J55, N80, L80, P110 Material (hu-steel.com)> Accessed 13/01/2021

[20] ATHMANI, S. "Étude des couches minces à base de terre rare destinées à la protection des matériaux contre la corrosion". Memoire Online (2013) Accessed 20/01/2021.

[21] C. Gabrielli, M. Keddam, A. Khalil, R. Rosset, M. Zidoune, Study of calcium carbonate scales by electrochemical impedance spectroscopy, Electrochimica Acta, Volume 42, Issue 8, 1997, Pages 1207-1218, ISSN 0013-4686, <https://doi.org/10.1016/S0013-4686(96)00289-7> . Accessed 10/02/2021

[22] C. Venâncio, J. Cavalcante Rocha, M. Cheriaf, "*Avaliação da Contaminação dos Metais Pesados em Matrizes Cimentícias por meio da Espectroscopia de Impedância Eletroquímica*". Doctoral Thesis 2017, UFSC Florianópolis Brazil - Accessed 16/02/2021.

[23] Mpelwa, M., Tang, SF. "*State of the art of synthetic threshold scale inhibitors for mineral scaling in the petroleum industry: a review*" Pet. Sci. 16, 830–849 (2019).<> Accessed 16/02/2021

[24] BK Giulini Safety Data Sheet, 2010. <http://www.burla.co.il/files/MSDS_FERROFOS_8441.pdf> Accessed 17/02/2021.

[25] Marín-Cruz, J., Cabrera-Sierra, R., Pech-Canul, M.A. et al. "*EIS characterization of the evolution of calcium carbonate scaling in cooling systems in presence of inhibitors*". J Solid State Electrochem 11, 1245–1252 (2007). Accessed 17/02/2021

[26] IRO Special Water Treatment Chemicals website, *HEDP – The Best Organic Phosphonic Anti Scale and Corrosion Inhibitor* and IRO Special Water Treatment Chemicals website, *Scale Inhibition Performance of PBTC andHEDP on CaCO3 Scale*, 2018 Accessed 18/02/202 2018

[27] Rayane Menzri, Samira Ghizellaoui, "*Chronoamperometry Study Of The Inhibition Of Groundwater Scaling Deposits In Fourchi*", Energy Procedia, Volume 18, 2012, Pages 1523-1532. - Accessed 19/02/2021

[28] H. Boufouchk, L. Delaplace, M. Desrieux, C. Sizaire. "*Practical Work - Medium Duration - Scaling of Steel*" INSA Lyon | January 2021 - Accessed 23/02/2021

[29] Köhl, Bernhard & Grundy, James & Baumann, Thomas. (2020). "Rippled scales in a geothermal facility in the Bavarian Molasse Basin: a key to understand the calcite scaling process". Geothermal Energy. 8. 10.1186/s40517-020-00177-6 - Accessed on 02/07/2022

[30] Schröder, H & Teschner, M & Köhler, Matthias & Seibt, A & Krüger, Martin & Friedrich, Analytik & Gbr, Bodenwasser Gesundheit & Gmbh, Geothermie. (2022). "Long term reliability of geothermal plants – Examples from Germany"- Accessed on 03/07/2022.

[31] Stanasel, Oana Delia et al. "Types of Scaling Occurring By Geothermal Utilization In A Low Température Geothermal Field" (2001) - Accessed on 04/07/2022.

[32] Jente Pauwels, Sonia Salah, Mirela Vasile, Ben Laenen, Valérie Cappuyns "Characterization of scaling material obtained from the geothermal power plant of the Balmatt site", Mol, Geothermics, Volume 94, 2021 - Accessed 04/07/2022

[33] "Chiffres clés des énergies renouvelables - Édition 2021" - Données et études statistiques Pour le changement climatique, l'énergie, l'environnement, le logement, et les transports - Accessed 01/08/2022

[34] "Brasil lidera transição energética no Brics" - IPEA - Instituto de Pesquisa Econômica Aplicada - Acessado em 01/08/2022

Annexes

Annexed Table 1: Detailed classification of geothermal fluids

Class	Preponderant State	TKS (ppm)	% of Chlorides	pH	Temperature
I	Liquid	> 100.000	99	< 5	~365°C
II	Liquid	500 - 60.000	15 - 99	< 4,5	> 200°C
III	Liquid	10.000 - 20.000	45 - 99	5 - 6	150 - 300°C
IV	Liquid	500 - 10.000	45 - 99	< 5	120 - 280°C
V - a	Liquid	<5.000	3 - 72	6,7 - 7,6	50 - 100°C
V - b	Liquid	< 5.000	3 - 72	7,8 - 9,85	120 - 200°C
VI	Vapor	< 1	-	-	160 - 250°C

Annexed Table 2: Composition of the main carbon steels used in Geothermal Power Plants in % of steel mass. [12][19]

Type	C	Mn	Mo	Cr	Ni	Cu	Ti	P	S	Si
L80	0,15 - 0,22	0,25 - 1,00	-	12 - 14	0,20	0,2	-	0,02	0,01	<1
N80	0,34 - 038	0,45 - 1,70	-	0,15	-	-	-	0,02	0,015	0,20 - 0,35
P110	0,26 - 0,40	0,40 - 0,70	0,15 - 0,25	0,8 - 1,1	0,2	0,2	-	0,02	0,02	0,17 - 0,37
Q125	0,35	1,35	0,85	1,5	0,99	-	-	0,02	0,01	-
P265GH	0,20	0,8 - 1,4	0,08	0,3	0,3	0,3	0,03	0,025	0,02	0,40
XC 38	0,32 - 0,39	0,5 - 0,8	-	-	-	-	-	<0,035	<0,035	0,3 - 0,4
XC 42	0,37 - 0,44	0,5 - 0,8	-	-	-	-	-	<0,035	<0,035	0,3 - 0,4

Annexed Table 3: Property to improve for each main type of alloying element added in stainless steels

Alloying Element	Property to be improved
Carbon (C)	The amount of carbon present in stainless steels is directly related to hardness. This is due to the formation of a solid solution and, at certain concentrations, to the formation of carbides.
Nickel (Ni)	Nickel will improve the mechanical properties of steels, as well as its corrosive properties.
Molybdenum (Mo)	Molybdenum has a great propensity for the formation of carbides. It increases creep resistance for low alloy steels. The addition of Mo is linked to the decrease in grain size and the improvement in mechanical and corrosive properties. High concentrations of Mo decrease the susceptibility of steels to pitting corrosion.
Copper (Cu)	Copper has a tendency to segregate. A concentration greater than 0,3% increases the mechanical properties for precipitation. It improves resistance to atmospheric corrosion. A concentration greater than 1% will increase the resistance to H_2SO4 and HCl.
Nitrogen (N)	Nitrogen is important for increasing the stability of the austenitic field. It can form nitrides and carbonitrides if V, Nb and Ti are present. It can cause precipitation or hardening by solid solution.
Chromium (Cr)	Chromium increases hardness, resistance to corrosion and oxidation.

Annexed Figure 1: First schematic drawing of the samples made by the mechanic workshop

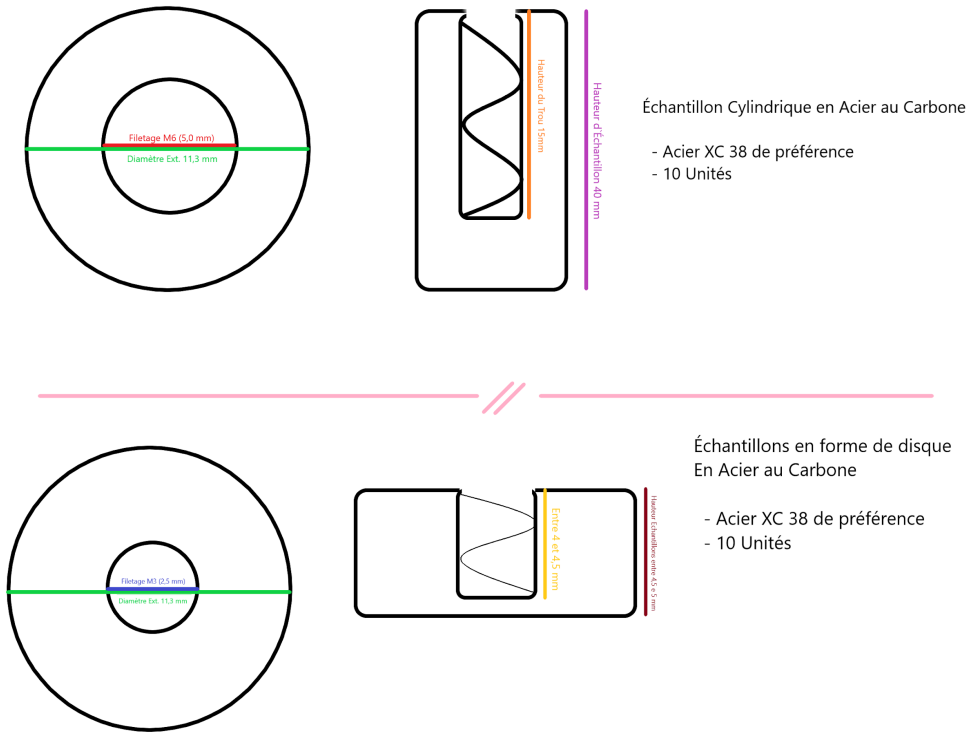

Annexed Figure 2: Photo of an overpolished sample

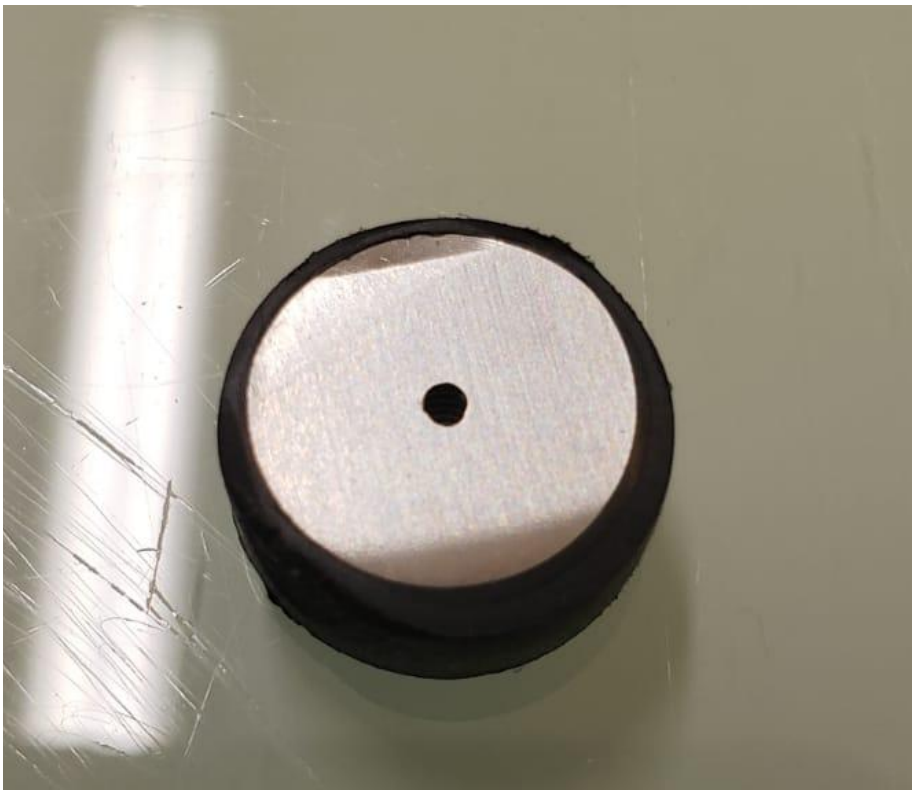

Annexed Figure 3: MEB Image of the hole caused by over polishing (XC42 Reference)

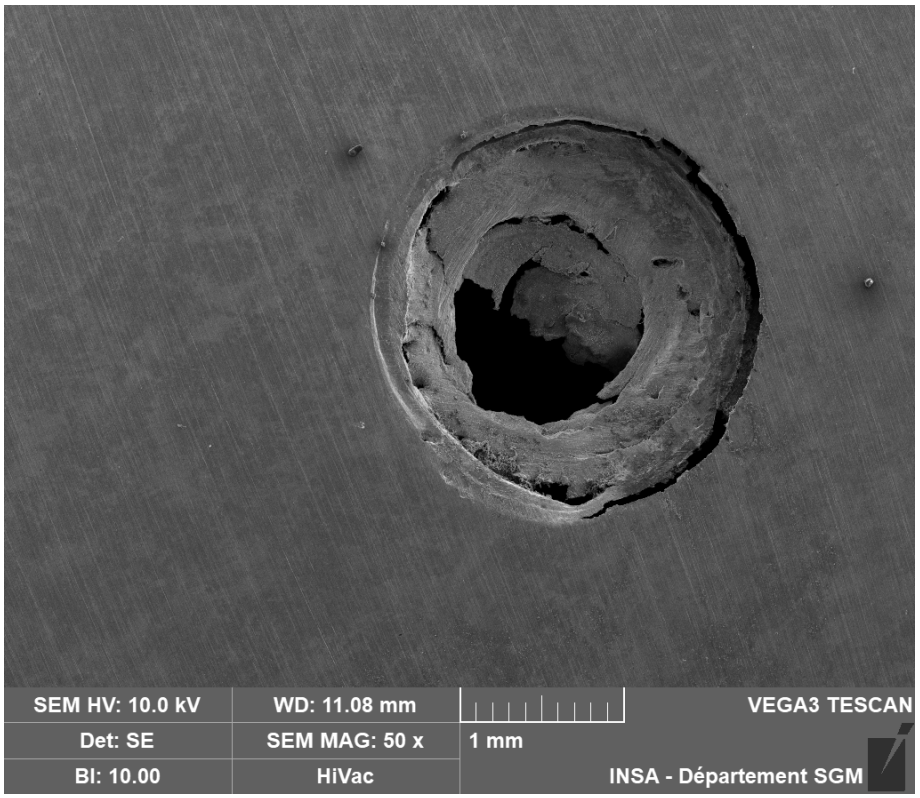

Annexed Figure 4: Pitting corrosion resistance polarization curve for 316L stainless steel in media with different concentrations of Cl.

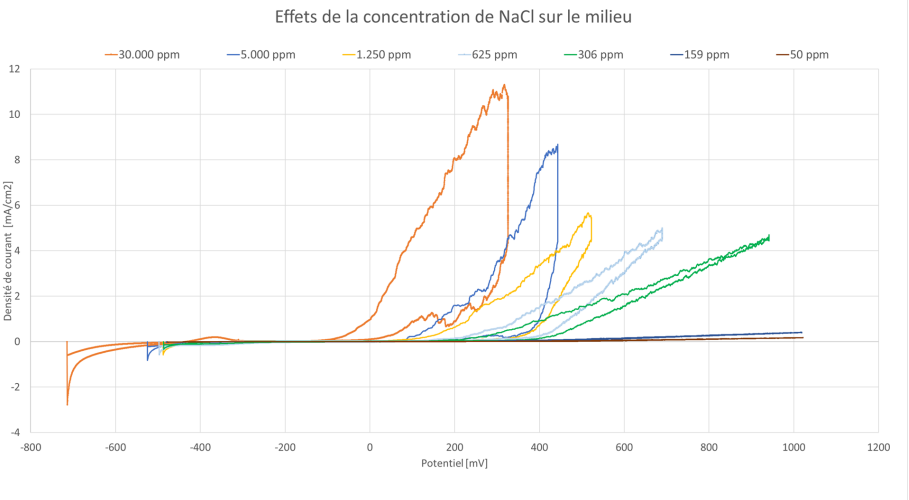

Annexed Figure 5: Accelerated Scaling of Stainless Steel 316L sample performed with Volvic Water (-0,7 $V_{Ag/AgCl}$)

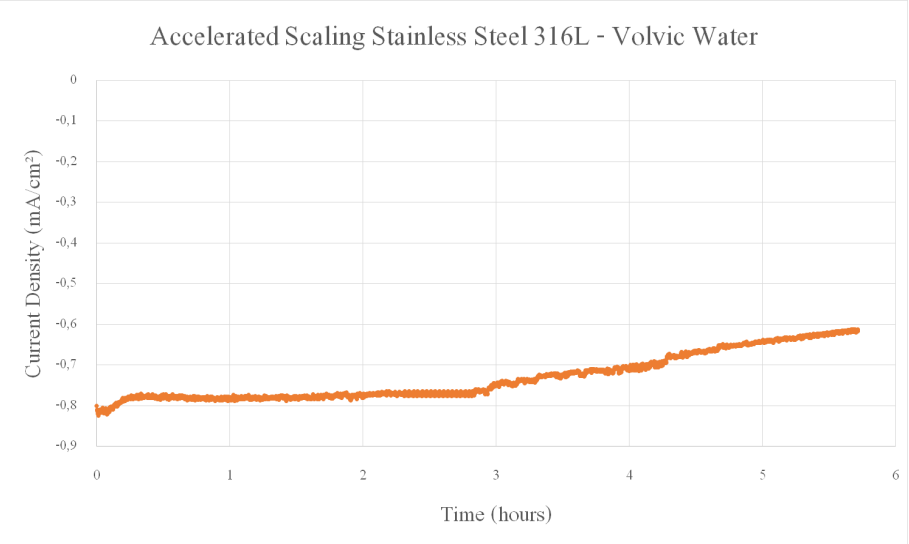

Annexed Figure 6: Comparative Accelerated Scaling Curves - 0,7 mg/L HEDP Solu II and TurboDispin 4363

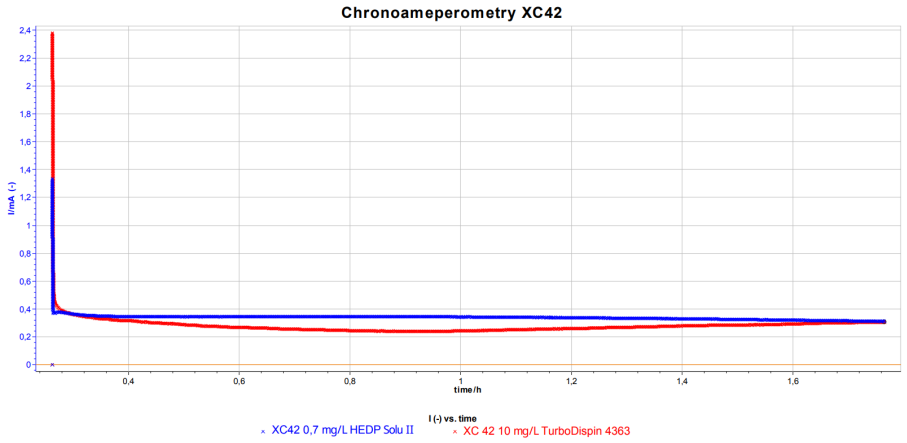

Annexed Figure 7: Nyquist Diagrams obtained from the Carbon Steel Samples

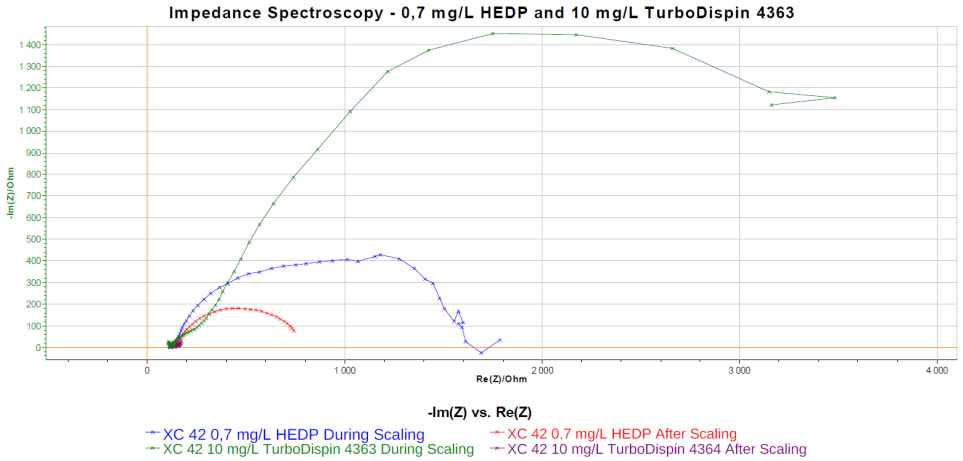

Annexed Figure 8: Carbon Steel Sample clearly corroded after experiment with 10 mg/L TurboDispin 4363